MICROPOROUS NETWORKS

Pore chemistry and size control in hybrid porous materials for acetylene capture from ethylene

Xili Cui,[1]* Kaijie Chen,[2]* Huabin Xing,[1]† Qiwei Yang,[1] Rajamani Krishna,[3] Zongbi Bao,[1] Hui Wu,[4] Wei Zhou,[4] Xinglong Dong,[5] Yu Han,[5] Bin Li,[6] Qilong Ren,[1] Michael J. Zaworotko,[2]† Banglin Chen[6]†

The trade-off between physical adsorption capacity and selectivity of porous materials is a major barrier for efficient gas separation and purification through physisorption. We report control over pore chemistry and size in metal coordination networks with hexafluorosilicate and organic linkers for the purpose of preferential binding and orderly assembly of acetylene molecules through cooperative host-guest and/or guest-guest interactions. The specific binding sites for acetylene are validated by modeling and neutron powder diffraction studies. The energies associated with these binding interactions afford high adsorption capacity (2.1 millimoles per gram at 0.025 bar) and selectivity (39.7 to 44.8) for acetylene at ambient conditions. Their efficiency for the separation of acetylene/ethylene mixtures is demonstrated by experimental breakthrough curves (0.73 millimoles per gram from a 1/99 mixture).

An urgent demand for efficient solutions to challenges in gas separation, sensing, and storage (*1*–*7*) has spurred research on custom-designed porous materials, termed metal-organic frameworks (MOFs) and/or porous coordination polymers (PCPs) (*8*), in which open lattices are formed from inorganic centers (nodes) and organic linking groups. These materials can be designed from first principles and, thanks to their inherent diversity, afford precise control over pore chemistry and pore size.

Ideal porous materials for gas separation should exhibit high selectivity and optimal adsorption capacity for the target gas molecules at relevant conditions. However, the design of new materials that improve upon existing benchmarks poses a daunting challenge to materials scientists (*9*–*12*). For example, porous materials are needed for acetylene (C_2H_2) capture and separation from ethylene (C_2H_4) (*13*–*17*), industrial processes that are relevant for the production of polymer-grade C_2H_2 and C_2H_4 (the most produced organic compound in the world, at over 140 million metric tons in 2014). The MOF-74 family of compounds has a high density of open metal sites that drive high uptake of C_2H_2 but displays low separation selectivities (*18*). The M′MOF (mixed metal–organic framework) family has ultramicropores that enable sieving effects and high separation selectivities but relatively low uptake of C_2H_2 (*19*).

We report that metal coordination networks with preformed inorganic and organic linkers—SIFSIX-2-Cu-i [SIFSIX, hexafluorosilicate (SiF_6^{2-}); 2, 4,4′-dipyridylacetylene; i, interpenetrated)] (*20*) and SIFSIX-1-Cu (1, 4,4′-bipyridine) (*21*)—can exhibit exceptional C_2H_2 capture performance because the geometric disposition of SiF_6^{2-} moieties enables preferential binding of C_2H_2 molecules. Both materials have pore spaces that enable extremely high C_2H_2 capture under low pressures, and they unexpectedly represent new benchmarks for the highly efficient removal of minor amounts of C_2H_2 from C_2H_4 gas (SIFSIX-2-Cu-i) and mass separation of C_2H_2/C_2H_4 mixtures under ambient conditions (SIFSIX-1-Cu). We attribute this unprecedented performance to the existence of "sweet spots" in pore chemistry and pore size that enable highly specific recognition and high uptake of C_2H_2 to occur in the same material.

In these SIFSIX materials, two-dimensional (2D) nets of organic ligand and metal node are pillared with SiF_6^- anions in the third dimension to form 3D coordination networks that have primitive cubic topology and, importantly, pore walls lined by inorganic anions (*20*–*23*). The pore sizes within this family of materials can be systematically tuned by changing the length of the organic linkers, the metal node, and/or the framework interpenetration. SIFSIX-1-Cu, SIFSIX-2-Cu, SIFSIX-2-Cu-i, SIFSIX-3-Cu (3, pyrazine), SIFSIX-3-Zn, and SIFSIX-3-Ni have already been studied for their exceptional CO_2 capture performance, but here we report a study of their C_2H_2 and C_2H_4 adsorption from 283 to 303 K. Figure 1, A and B, and figs. S2 to S7 show dramatically different adsorption behaviors for C_2H_2 than those observed for CO_2 (figs. S8 and S9) (*24*). SIFSIX-2-Cu-i rapidly adsorbs C_2H_2 at very low pressure (≤0.05 bar). Its C_2H_2 uptake reaches 2.1 mmol/g at 298 K and 0.025 bar (Fig. 1B), compared with an uptake of 1.78 mmol/g by UTSA-100a (*17*). This performance at low pressure indicates that SIFSIX-2-Cu-i has promise for capturing C_2H_2 when it is a minor component in a gas mixture. SIFSIX-1-Cu exhibits exceptionally high C_2H_2 uptake (8.5 mmol/g) at 298 K and 1.0 bar. This is not only the highest uptake of any of the SIFSIX materials, but is also even higher than that of the previous benchmark, FeMOF-74 (table S1) (*18*, *24*). As detailed herein, we attribute the unprecedented performance of these materials to their hybrid pore chemistry and optimal pore sizes for binding C_2H_2.

To understand the C_2H_2 adsorption isotherms in these materials, we conducted detailed modeling studies using first-principles DFT-D (dispersion-corrected density functional theory) calculations. In SIFSIX-1-Cu, C_2H_2 molecules are bound through strong C–H···F hydrogen (H) bonding (2.017 Å) and van der Waals (vdW) interactions with the 4,4′-bipyridine linkers (Fig. 1C and fig. S10) (*24*). The DFT-D–calculated static adsorption energy (ΔE) is 44.6 kJ/mol. Each unit cell of SIFSIX-1-Cu contains four equivalent exposed F atoms, and each exposed F atom binds one C_2H_2 molecule. The distance between neighboring adsorbed C_2H_2 molecules is ideal for them to synergistically interact with each other through multiple $H^{\delta+}\cdots C^{\delta-}$ dipole-dipole interactions (Fig. 1C), further enhancing the energy of adsorption. Because four C_2H_2 molecules are adsorbed per unit cell, the ΔE of C_2H_2 increases to 47.0 kJ/mol. The strong binding of C_2H_2 at F atoms and the geometric arrangement of SiF_6^{2-} anions enable the efficient packing of four C_2H_2 molecules per unit cell and very high C_2H_2 uptake at 298 K and 1.0 bar (about 4.4 C_2H_2 molecules per unit cell).

C_2H_2 adsorption is weaker in the wider-pore material SIFSIX-2-Cu (10.5 Å × 10.5 Å cavity) than in SIFSIX-1-Cu (ΔE, 34.6 versus 44.6 kJ/mol; uptake, 5.3 versus 8.5 mmol/g). The C–H···F H-bonding interaction from SiF_6^{2-} sites is of the same nature in these isoreticular networks (Fig. 1, C and D). However, the vdW interaction between C_2H_2 and the organic linker in SIFSIX-2-Cu is weak compared with that in SIFSIX-1-Cu. We attribute this difference to the former's larger pore size and weaker vdW potential overlap (figs. S10 and S11) (*24*). Moreover, at high gas uptake, the C_2H_2 molecules adsorbed on adjacent F sites are too far separated to have synergistic guest-guest interactions. However, in the twofold interpenetrated structure of SIFSIX-2-Cu-i, one C_2H_2 molecule can be simultaneously bound by two F atoms from different nets through cooperative C–H···F H-bonding (2.013 and 2.015 Å; Fig. 1E), which enables the strongest energy of C_2H_2 binding yet observed in SIFSIX materials (ΔE, 52.9 kJ/mol). The strong adsorption energy of SIFSIX-2-Cu-i contributes to its extremely high uptake capacity at low pressure. In SIFSIX-3-Zn and SIFSIX-3-Ni, which are

[1]Key Laboratory of Biomass Chemical Engineering of Ministry of Education, College of Chemical and Biological Engineering, Zhejiang University, Hangzhou 310027, China. [2]Department of Chemical and Environmental Sciences, University of Limerick, Limerick, Republic of Ireland. [3]Van 't Hoff Institute for Molecular Sciences, University of Amsterdam, Science Park 904, 1098 XH Amsterdam, Netherlands. [4]Center for Neutron Research, National Institute of Standards and Technology, Gaithersburg, MD 20899-6102, USA. [5]Advanced Membranes and Porous Materials Center, Physical Sciences and Engineering Division, King Abdullah University of Science and Technology, Thuwal 23955-6900, Saudi Arabia. [6]Department of Chemistry, University of Texas–San Antonio, One UTSA Circle, San Antonio, TX 78249-0698, USA.

*These authors contributed equally to this work. †Corresponding author. Email: xinghb@zju.edu.cn (H.X.); michael.zaworotko@ul.ie (M.J.Z.); banglin.chen@utsa.edu (B.C.)

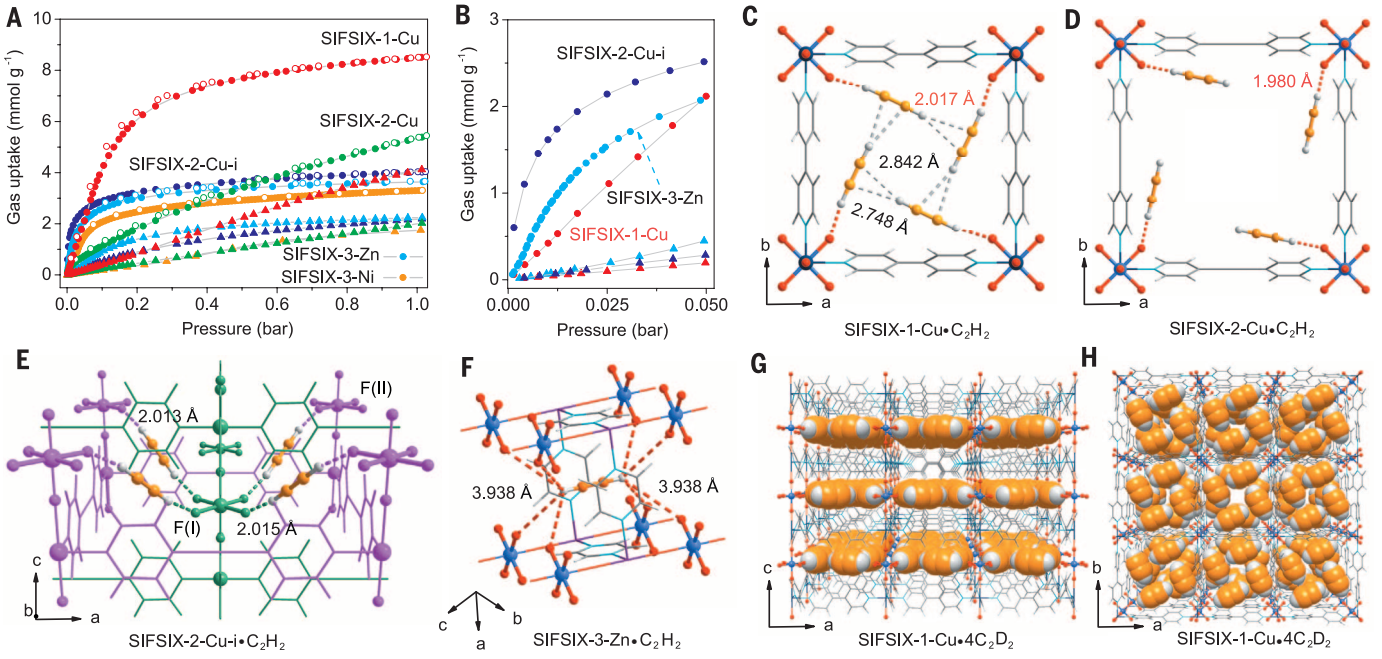

Fig. 1. C_2H_2 and C_2H_4 adsorption isotherms of the MOFs, DFT-D–simulated optimized C_2H_2 adsorption sites of the MOFs, and neutron crystal structure of SIFSIX-1-Cu·4C_2D_2. (**A** and **B**) Adsorption isotherms of C_2H_2 (filled circles) and C_2H_4 (triangles) in SIFSIX-1-Cu (red), SIFSIX-2-Cu (green), SIFSIX-2-Cu-i (blue), SIFSIX-3-Zn (light blue), and SIFSIX-3-Ni (orange) at 298 K in two pressure regions, 0 to 1.0 bar (A) and 0 to 0.05 bar (B). Open circles in (A) are desorption isotherms of C_2H_2 (**C** to **F**) DFT-D–calculated C_2H_2 adsorption binding sites in SIFSIX-1-Cu (C), SIFSIX-2-Cu (D), SIFSIX-2-Cu-i (E) (the different nets are highlighted in magenta and green for clarity), and SIFSIX-3-Zn (F). Color code: F, red; Si, light blue; C, gray; H, light gray; N, sky blue; Cu, dark teal; Zn, violet; C (in C_2H_2 or C_2D_2), orange. (**G** and **H**) Neutron crystal structure of SIFSIX-1-Cu·4C_2D_2 at 200 K, determined from Rietveld analysis.

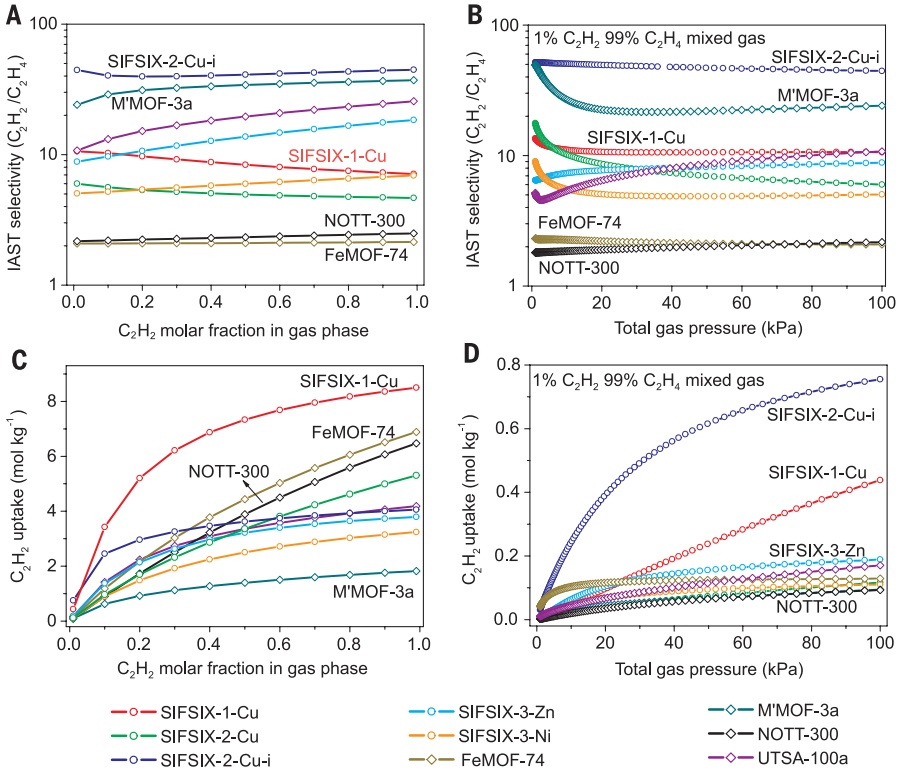

Fig. 2. IAST calculations for MOF performance with C_2H_2/C_2H_4 mixtures. (**A** and **B**) Comparison of the IAST selectivities of SIFSIX materials versus those of previously reported best-performing materials for C_2H_2/C_2H_4 mixtures. Results for varying C_2H_2 molar fractions at 100 kPa are shown in (A), and results at varying pressures for a 1% C_2H_2 mixture are shown in (B). (**C** and **D**) MOF capacity to uptake C_2H_2 from C_2H_2/C_2H_4 mixtures. Results for varying C_2H_2 molar fractions at 100 kPa are shown in (C), and results at varying pressures for a 1% C_2H_2 mixture are shown in (D).

the strongest CO_2 adsorbents, the pore size is smallest, and C_2H_2 molecules are primarily adsorbed at a different site in the 1D channel along the *c* axis (ΔE, 50.3 kJ/mol; Fig. 1F). The secondary adsorption site in SIFSIX-3-Zn (fig. S12) (*24*) exhibits a much smaller adsorption energy (25.9 kJ/mol), which results in lower C_2H_2 uptake compared with that of SIFSIX-2-Cu-i.

The weakly basic nature of the SiF_6^{2-} sites (acid dissociation constant pK_a, 1.92) and their geometric disposition enable strong binding with weakly acidic C_2H_2 molecules. Because C_2H_2 is more acidic than C_2H_4 (pK_a, 25 versus 44) (*17*), and the geometry of the SIFSIX materials is more optimal for C_2H_2 binding, there are much stronger interactions with C_2H_2 than with C_2H_4 (ΔE in SIFSIX-1-Cu, 44.6 versus 27.2 kJ/mol; ΔE in SIFSIX-2-Cu-i, 52.9 versus 39.8 kJ/mol). The calculated H-bond distances between C_2H_4 and SiF_6^{2-} sites are 2.541 and 2.186 Å in SIFSIX-1-Cu and SIFSIX-2-Cu-i, respectively, which are longer than those between C_2H_2 and SiF_6^{2-} sites (figs. S13 and S14) (*24*).

To establish the structure of the C_2H_2 binding sites through Rietveld structural refinements, high-resolution neutron powder diffraction data were collected on C_2D_2-loaded samples of SIFSIX-1-Cu·4C_2D_2 and SIFSIX-2-Cu-i·1.7C_2D_2 at 200 K (figs. S15 and S16) (*24*). Each unit cell of SIFSIX-1-Cu is filled with four C_2D_2 molecules that are arranged in an ordered planar structure (Fig. 1, G and H), consistent with the DFT-D modeling results. C–D···F H-bonding occurs between C_2D_2 and SiF_6^- anions (2.063 Å), and $D^{\delta+}\cdots C^{\delta-}$ distances between neighboring C_2D_2 molecules are 3.063 and 3.128 Å. In SIFSIX-2-Cu-i, each C_2H_2

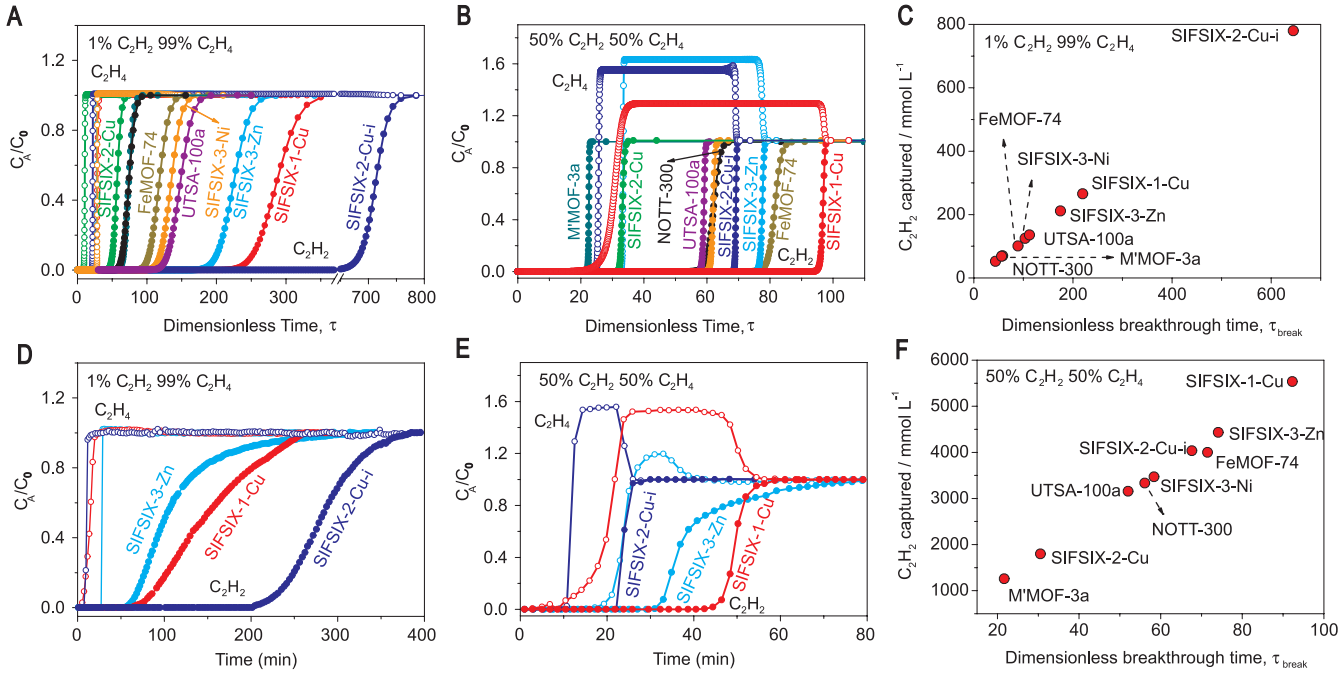

Fig. 3. Simulated and experimental column breakthrough results. (**A** and **B**) Simulated column breakthrough curves for C_2H_2/C_2H_4 separations with SIFSIX materials and previously reported best-performing materials [(A), 1/99 mixture; (B), 50/50 mixture]. (**C** and **F**) Plots of the amount of C_2H_2 captured as a function of τ_{break} in the simulated column breakthrough [(C), 1/99 mixture; (F), 50/50 mixture]. (**D** and **E**) Experimental column breakthrough curves for C_2H_2/C_2H_4 separations with SIFSIX-1-Cu, SIFSIX-2-Cu, and SIFSIX-3-Zn at 298 K and 1.01 bar [(D), 1/99 mixture; (E), 50/50 mixture]. In (A), (B), (D), and (E), open circles are for C_2H_4, and filled circles are for C_2H_2. C_A/C_0, outlet concentration/feed concentration.

interacts with two SiF_6^- anions via dual C–D···F H-bonding (2.134 Å; fig. S17) (*24*).

The separation of C_2H_2 from C_2H_4 is necessary for the production of high-purity C_2H_4 and C_2H_2. In the production of polymer-grade C_2H_4, removal of trace C_2H_2 (about 1%) from C_2H_4 gas must meet the requirement of <40 parts per million (ppm) C_2H_2 in the downstream polymerization reaction (*17*). Similarly, in the production of polymer-grade C_2H_2 by pyrolysis of coal and biomass, the capture of C_2H_2 from C_2H_2/C_2H_4 mixtures (90/10 to 50/50, v/v) is a crucial step. Existing methods, such as solvent absorption and partial hydrogenation of C_2H_2 (*25*), are energy intensive, so there is an urgent need to develop efficient porous materials for C_2H_2 capture from C_2H_4.

To address gas mixture separations, we first determined the C_2H_2/C_2H_4 separation selectivities of the SIFSIX materials by means of ideal adsorbed solution theory (IAST) calculations (Fig. 2 and fig. S20) (*24*, *26*). SIFSIX-2-Cu-i exhibits record C_2H_2/C_2H_4 selectivities (39.7 to 44.8; Fig. 2A), even greater than those of M'MOF-3a (table S1). Because SIFSIX-2-Cu-i adsorbs a high amount of C_2H_2 under very low pressures, it not only has the highest C_2H_2/C_2H_4 selectivities (Fig. 2B) but also the highest C_2H_2 uptake (Fig. 2D) for C_2H_2/C_2H_4 (1/99) mixtures. SIFSIX-1-Cu displays moderately high C_2H_2/C_2H_4 separation selectivities (7.1 to 10.6), which are greater than those of FeMOF-74 (2.1) (*18*) and NOTT-300 (2.2 to 2.5) (*14*) (Fig. 2A). For C_2H_2/C_2H_4 (1/99) mixtures, SIFSIX-1-Cu exhibits greater selectivities (10.6) than SIFSIX-3-Zn (8.8) and SIFSIX-3-Ni (5.0) (Fig. 2B). Its C_2H_2 uptake from the 1/99 mixture is the second highest of the compounds investigated (Fig. 2D). Given that SIFSIX-1-Cu has a relatively large surface area, it should also be very efficient for C_2H_2/C_2H_4 (1/99) separation. SIFSIX-1-Cu exhibits higher C_2H_2 uptakes than benchmark MOFs, including FeMOF-74, NOTT-300, and UTSA-100a. Its high C_2H_2/C_2H_4 selectivities (Fig. 2A) make SIFSIX-1-Cu most suitable for C_2H_2/C_2H_4 (50/50) separation (Fig. 2C and fig. S20) (*24*). Some further comparisons of how these MOFs perform with respect to C_2H_2/C_2H_4 separations are shown in table S1 (*24*).

Transient breakthrough simulations (*27*) were conducted to demonstrate the C_2H_2/C_2H_4 separation performances of the SIFSIX materials in column adsorption processes. Two C_2H_2/C_2H_4 mixtures (1/99 and 50/50) were used as feeds to mimic the industrial process conditions. Clean separations were realized with all five SIFSIX MOFs; C_2H_4 first eluted through the bed to yield a polymer-grade gas, then C_2H_2 broke through from the bed at a certain time τ_{break} (Fig. 3A and figs. S21 and S22) (*24*). The dimensionless τ_{break} values for SIFSIX-1-Cu (1/99 and 50/50 mixtures) and SIFSIX-2-Cu-i (1/99 mixture) exceed those of the other SIFSIX materials and MOFs that we studied (Fig. 3, A and B). The amount of C_2H_2 captured from the 1/99 mixture in SIFSIX-1-Cu and SIFSIX-2-Cu-i was as high as 265.3 and 780.0 mmol/liter, respectively, which compares favorably with state-of-art adsorbents such as UTSA-100a (135.5 mmol/liter), FeMOF-74 (100.7 mmol/liter), and NOTT-300 (68.3 mmol/liter). SIFSIX-2-Cu-i efficiently removes trace C_2H_2 from C_2H_4 gas (1/99 mixture), whereas SIFSIX-1-Cu demonstrates excellent C_2H_2 capacity with an uptake of 5533 mmol/liter from the 50/50 mixture, ~37% greater than that of FeMOF-74 (Fig. 3F).

Through experimental breakthrough studies, we further examined these materials in actual adsorption processes for both 1/99 and 50/50 mixtures. Highly efficient separations for C_2H_2/C_2H_4 mixtures were realized (Fig. 3, D and E). For the capture of C_2H_2 from the 1/99 mixture, the concentration of C_2H_2 in the gas exiting the adsorber for up to 140 min was below 2 ppm, and the purity of C_2H_4 was >99.998% (fig. S23) (*24*). The hierarchy of breakthrough times for the 1/99 mixture was, from longest to shortest, SIFSIX-2-Cu-i, SIFSIX-1-Cu, then SIFSIX-3-Zn; for the 50/50 mixture, it was SIFSIX-1-Cu, SIFSIX-3-Zn, then SIFSIX-2-Cu-i (Fig. 3, D and E). These experiments are consistent with simulated breakthrough results. Although the uptake of C_2H_2 by SIFSIX-3-Zn at low pressure for the 1/99 mixture is higher than that by SIFSIX-1-Cu (Fig. 1B), SIFSIX-1-Cu exhibits a longer breakthrough time for C_2H_2, presumably because of its higher selectivity (Fig. 2B). The amounts of C_2H_2 captured by SIFSIX-1-Cu, SIFSIX-2-Cu-i, and SIFSIX-3-Zn from the 1/99 mixture (0.38, 0.73, and 0.08 mmol/g, respectively) and from the 50/50 mixture (6.37, 2.88, and 1.52 mmol/g, respectively) during the breakthrough process are in excellent agreement with the simulated results, except in the case of SIFSIX-3-Zn (tables S12 and S13) (*24*).

In the production of high-purity C_2H_4, the feed gases for the C_2H_2 removal unit are contaminated with trace levels of CO_2 (<50 ppm), H_2O (<5 ppm), and O_2 (<5 ppm). We conducted breakthrough experiments for the 1/99 mixture with SIFSIX-2-Cu-i, the best-performing material for capturing trace

amounts of C_2H_2. These experiments indicate that the presence of CO_2 has only a slight (1000 ppm CO_2) or no (10 ppm CO_2) effect on the separation of C_2H_2 from C_2H_4 (fig. S24) (*24*). Moisture (6 to 1340 ppm) and oxygen (2200 ppm) do not affect the C_2H_2 capture ability of SIFSIX-2-Cu-i (figs. S25 and S26) (*24*). The breakthrough performances of SIFSIX-2-Cu-i and SIFSIX-3-Zn for the 1/99 mixture did not decline during 16 and 3 cycles, respectively (figs. S28 and S29) (*24*), and the SIFSIX materials retained their stability after breakthrough experiments (figs. S1 and S30) (*24*).

The SIFSIX materials that we studied exhibit excellent C_2H_2 storage performance. The volumetric uptake of C_2H_2 by SIFSIX-1-Cu at 298 K and 1.0 bar is the highest among these SIFSIX materials (0.191 g/cm^3; table S14) (*24*). The C_2H_2 storage densities in the pores of SIFSIX-1-Cu, SIFSIX-2-Cu-i, and SIFSIX-3-Zn at 298 K are 0.388, 0.403, and 0.499 g/cm^3, respectively.

The basic principles outlined here are likely to be applicable to other gas mixtures. Primary binding sites will be necessary for recognition of specific gas molecules, whereas suitable pore sizes and spacing will be needed to enforce synergistic binding to multiple sites in order to form the so-called "gas clusters" through intermolecular guest-guest interactions. This work not only reveals a path forward for industrial C_2H_2/C_2H_4 separations, but also facilitates a design or crystal engineering approach to the development of porous materials for other gas separations.

REFERENCES AND NOTES

1. S. Kitagawa, *Angew. Chem. Int. Ed.* **54**, 10686–10687 (2015).
2. R. Vaidhyanathan *et al.*, *Science* **330**, 650–653 (2010).
3. N. T. T. Nguyen *et al.*, *Angew. Chem. Int. Ed.* **53**, 10645–10648 (2014).
4. N. L. Rosi *et al.*, *Science* **300**, 1127–1129 (2003).
5. Y. Peng *et al.*, *J. Am. Chem. Soc.* **135**, 11887–11894 (2013).
6. J. A. Mason *et al.*, *Nature* **527**, 357–361 (2015).
7. S. Ma *et al.*, *J. Am. Chem. Soc.* **130**, 1012–1016 (2008).
8. H. Furukawa, K. E. Cordova, M. O'Keeffe, O. M. Yaghi, *Science* **341**, 1230444 (2013).
9. S. J. Datta *et al.*, *Science* **350**, 302–306 (2015).
10. Z. J. Zhang, Z.-Z. Yao, S. Xiang, B. Chen, *Energy Environ. Sci.* **7**, 2868–2899 (2014).
11. Q. Lin, T. Wu, S. T. Zheng, X. Bu, P. Feng, *J. Am. Chem. Soc.* **134**, 784–787 (2012).
12. J.-R. Li, R. J. Kuppler, H.-C. Zhou, *Chem. Soc. Rev.* **38**, 1477–1504 (2009).
13. R. Matsuda *et al.*, *Nature* **436**, 238–241 (2005).
14. S. Yang *et al.*, *Nat. Chem.* **7**, 121–129 (2014).
15. H. Wu, Q. Gong, D. H. Olson, J. Li, *Chem. Rev.* **112**, 836–868 (2012).
16. J.-P. Zhang, X.-M. Chen, *J. Am. Chem. Soc.* **131**, 5516–5521 (2009).
17. T. L. Hu *et al.*, *Nat. Commun.* **6**, 7328–7335 (2015).
18. E. D. Bloch *et al.*, *Science* **335**, 1606–1610 (2012).
19. M. C. Das *et al.*, *J. Am. Chem. Soc.* **134**, 8703–8710 (2012).
20. P. Nugent *et al.*, *Nature* **495**, 80–84 (2013).
21. S. Noro *et al.*, *J. Am. Chem. Soc.* **124**, 2568–2583 (2002).
22. O. Shekhah *et al.*, *Nat. Commun.* **5**, 4228–4234 (2014).
23. A. Kumar *et al.*, *Angew. Chem. Int. Ed.* **54**, 14372–14377 (2015).
24. Materials and methods are available as supplementary materials on *Science* Online.
25. F. Studt *et al.*, *Science* **320**, 1320–1322 (2008).
26. K. S. Walton, D. S. Sholl, *AIChE J.* **61**, 2757–2762 (2015).
27. R. Krishna, *RSC Adv.* **5**, 52269–52295 (2015).

ACKNOWLEDGMENTS

This work is supported by the National Natural Science Foundation of China (grants 21222601, 21436010, and 21476192), Zhejiang Provincial Natural Science Foundation of China (grant LR13B060001), Ten Thousand Talent Program of China (to H.X.), the Welch Foundation (grant AX-1730), King Abdullah Science and Technology University Office of Competitive Research Funds (grant URF/1/1672-01-01), and the Science Foundation Ireland (award 13/RP/B2549 to M.Z.). We thank T. L. Hu, Y. F. Zhao, W. D. Shan, and M. D. Jiang for their help and arrangement of the breakthrough experiments; A. Kumar for help with sample characterization; and Z. G. Zhang and B. G. Su for discussions of the experiments. Metrical data for the solid-state structures of SIFSIX-2-Cu-i·C_2D_2 and SIFSIX-1-Cu·C_2D_2 are available free of charge from the Cambridge Crystallographic Data Centre under reference numbers CCDC 1471795 and 1471796.

The authors and their affiliated institutions have filed a patent application related to the results presented here.

SUPPLEMENTARY MATERIALS

www.sciencemag.org/content/353/6295/141/suppl/DC1
Materials and Methods
Figs. S1 to S32
Tables S1 to S15
References (*28*–*34*)

12 January 2016; accepted 5 May 2016
Published online 19 May 2016
10.1126/science.aaf2458

ORGANIC CHEMISTRY

Copper-catalyzed asymmetric addition of olefin-derived nucleophiles to ketones

Yang Yang,[1] Ian B. Perry,[1] Gang Lu,[2] Peng Liu,[2]* Stephen L. Buchwald[1]*

Enantioenriched alcohols found in an array of bioactive natural products and pharmaceutical agents are often synthesized by asymmetric nucleophilic addition to carbonyls. However, this approach generally shows limited functional-group compatibility, requiring the use of preformed organometallic reagents in conjunction with a stoichiometric or substoichiometric amount of chiral controller to deliver optically active alcohols. Herein we report a copper-catalyzed strategy for the stereoselective nucleophilic addition of propargylic and other alkyl groups to ketones, using easily accessible (poly)unsaturated hydrocarbons as latent carbanion equivalents. Our method features the catalytic generation of highly enantioenriched organocopper intermediates and their subsequent diastereoselective addition to ketones, allowing for the effective construction of highly substituted stereochemical dyads with excellent stereocontrol. Moreover, this process is general, scalable, and occurs at ambient temperature.

Stereochemically complex alcohols in optically pure form are commonly encountered structural elements in a diverse range of pharmaceutical drugs and biologically active natural products (Fig. 1A). Consequently, general methods that allow for the stereoselective assembly of highly substituted alcohols have long been sought (*1*). The discovery of Grignard reagents and their subsequent addition to ketones and aldehydes have been widely considered as milestones in synthetic chemistry, giving rise to a general synthesis of alcohols from preformed organomagnesium reagents and broadly available carbonyl compounds (*2*). Since then, extensive efforts have been devoted to the development of asymmetric variants of nucleophilic addition reactions to carbonyls, using preformed organometallic reagents (*1*, *3*–*7*). These synthetic endeavors have proven to be exceptionally fruitful, culminating in a variety of protocols for enantioselective additions to carbonyls, using either a chiral auxiliary-modified organometallic reagent or a substoichiometric amount of chiral controller to achieve excellent levels of stereocontrol. Compared with aldehydes, however, the asymmetric nucleophilic addition to ketones has been studied to a lesser extent (*5*–*7*).

Although numerous advances have been made in this area, considerable hurdles have impeded the further adaptation of these methods by the synthetic community. The requirement to prepare and use a stoichiometric quantity of an organometallic reagent complicates most of the existing methods. In addition, the highly nucleophilic and basic nature of organometallic reagents has posed substantial limitations with respect to the functional-group compatibility of these processes. As a consequence, these methods are typically not amenable to the transformation of late-stage intermediates and other highly functionalized molecules. Furthermore, an additional synthetic operation is required to prepare these organometallic reagents from organic halide or unsaturated hydrocarbon precursors, imposing further constraints on the types of nucleophiles suitable for carbonyl addition.

In this context, a catalytic method for stereoselective additions to carbonyls, using easily accessible olefins as latent carbanion equivalents in

[1]Department of Chemistry, Massachusetts Institute of Technology (MIT), Cambridge, MA 02139, USA. [2]Department of Chemistry, University of Pittsburgh, Pittsburgh, PA 15260, USA.
*Corresponding author. Email: pengliu@pitt.edu (P.L.); sbuchwal@mit.edu (S.L.B.)

Editor's Summary

Separating one organic from another

Separating closely related organic molecules is a challenge (see the Perspective by Lin).The separation of acetylene from ethylene is needed in high-purity polymer production. Cui et al. developed a copper-based metal-organic framework with hexafluorosilicate and organic linkers designed to have a high affinity for acetylene. These materials, which capture four acetylene molecules in each pore, successfully separated acetylene from mixtures with ethylene. Propane and propylene are both important feedstock chemicals. Their physical and chemical similarity, however, requires energy-intense processes to separate them. Cadiau et al. designed a fluorinated porous metal-organic framework material that selectively adsorbed propylene, with the complete exclusion of propane.

Science, this issue pp. 141 and 137; see also p. 121

www.sciencemag.org/cgi/content/full/science.aaf3458/DC1

Supplementary Materials for

Pore chemistry and size control in hybrid porous materials for acetylene capture from ethylene

Xili Cui,* Kaijie Chen,* Huabin Xing,† Qiwei Yang, Rajamani Krishna, Zongbi Bao, Hui Wu, Wei Zhou, Xinglong Dong, Yu Han, Bin Li, Qilong Ren, Michael J. Zaworotko,† Banglin Chen†

*These authors contributed equally to this work.
†Corresponding author. Email: xinghb@zju.edu.cn (H.X.); michael.zaworotko@ul.ie (M.J.Z.); banglin.chen@utsa.edu (B.C.)

Published 19 May 2016 on *Science* First Release
DOI: 10.1126/science.aaf2458

This PDF file includes:

Materials and Methods
Figs. S1 to S32
Tables S1 to S15
Full Reference List

Materials and Methods

Materials

Ammonium hexafluorosilicate ($(NH)_2SiF_6$, 98%, Aldrich), copper (II) tetrafluoroborate hydrate ($Cu(BF_4)_2$• xH_2O, 98%, Aldrich), zinc hexafluorosilicate hydate ($ZnSiF_6$• xH_2O, 99%, Aldrich), 4,4'-bipyridine ($C_{10}H_8N_2$, 98%, Aldrich), 4-(2-pyridin-4-ylethynyl)pyridine ($C_{12}H_8N_2$, 98%, Chemsoon), pyrazine ($C_4H_4N_2$, 99%, Aldrich), methanol (CH_3OH, anhydrous, 99%, Sigma-Aldrich), ethylene glycol ($C_2H_6O_2$, anhydrous, 99%, Sigma-Aldrich), were purchased and used without further purification.

N_2 (99.999%), C_2H_2 (99%), C_2H_4 (99.99%), He (99.999%) and mixed gases of (1) C_2H_2/C_2H_4 = 1/99 (v/v), (2) C_2H_2/C_2H_4 = 50/50 (v/v), (3) 100 ppm CO_2, 1% C_2H_2 and 98.99% C_2H_4; (4) 1000 ppm CO_2, 1% C_2H_2 and 98.9% C_2H_4 were purchased form JinGong Company (China). Mixed gases of (5) 6 ppm H_2O, 1% C_2H_2 and 98.99% C_2H_4, (6) 83 ppm H_2O, 1% C_2H_2 and 98.99% C_2H_4, (7) 1340 ppm H_2O, 1% C_2H_2, and 98.86% C_2H_4, and standard gases of C_2H_2 and C_2H_4 were purchased form Shanghai Wetry Standard Reference Gas Analytical Technology Co. LTD (China).

Methods

Synthesis of SIFSIX-1-Cu (Cu(4,4'-bipyridine)$_2$SiF$_6$•8H$_2$O)n

Firstly, 0.35 g 4,4'-bipyridine was dissolved in 40 mL ethylene glycol at 338 K. An aqueous solution (20 mL) of $Cu(BF_4)_2$•xH_2O (266 mg, 1.12 mmol) and $(NH_4)_2SiF_6$ (199 mg, 1.12 mmol) was added to the above solution. Then the mixture was heated at 65 ℃ for 3 h under stirring. The obtained purple powder was filtered, washed with methanol, and was exchanged with methanol for 3 days. (*21*)

Synthesis of SIFSIX-2-Cu (Cu(4,4'-bipyridylacetylene)$_2$SiF$_6$)n

An ethanol solution (2.0 mL) of 4,4'-bipyridylacetylene (0.115mmol) was carefully layered onto an ethylene glycol solution (2.0 mL) of $CuSiF_6$•xH_2O (0.149 mmol). Crystals of SIFSIX-2-Cu were obtained after two weeks. The obtained sample was exchanged with ethanol for 4 days. (*20*)

Synthesis of SIFSIX-2-Cu-i (Cu(4,4'-bipyridylacetylene)$_2$SiF$_6$).

A methanol solution (4.0 mL) of 4,4'-bipyridylacetylene (0.286 mmol) was mixed with an aqueous solution (4.0 mL) of $Cu(BF_4)_2$•xH_2O (0.26 mmol) and $(NH_4)_2SiF_6$ (0.26 mmol) and then heated at 85 ℃ for 12 h. The obtained sample was exchanged with methanol for 3 days. (*20*)

Synthesis of SIFSIX-3-Zn (Zn(pyrazine)$_2$SiF$_6$)n

A methanol solution (2.0 mL) of pyrazine (1.3mmol) was carefully layered onto a methanol solution (2.0 mL) of $ZnSiF_6$• xH_2O (0.13 mmol). Colourless crystals of SIFSIX-3-Zn were obtained after two days. The obtained sample was exchanged with ethanol for 1 days. (*20*)

Synthesis of SIFSIX-3-Ni (Ni(pyrazine)$_2$SiF$_6$)n

A methanol solution (20 ml) of nickel silicofluoride, $NiSiF_6$ (1mmol) and pyrazine (2mmol) was mixed and heated at 85 ℃. Blue powder was obtioned after 3days. The obtained sample was exchanged with ethanol for 3 days. (*23*)

Synthesis of SIFSIX-3-Cu (Cu(pyrazine)$_2$SiF$_6$)n

A hot methanol solution (10 mL) of pyrazine (2 mmol) was slowly added into a hot methanol solution (10 mL) of $CuSiF_6$•H_2O (1 mmol). The blue precipitate immoderately was obtained and

suspended in the solution. After stirring this mixture for 1 minute, SIFSIX-3-Cu was harvested by direct filtration. Attention: longer stirring time will introduce more impurity. The sample was then dried in the air and degassed under high vacuum at 50 ℃ for 12 hours before used for sorption experiments. (*22*)

Pure gas adsorpiton

SIFSIX-1-Cu, SIFSIX-2-Cu, SIFSIX-2-Cu-i, and SIFSIX-3-Zn were evacuated at room temperature for 1-2 days until the pressure dropped below 7μm Hg. SIFSIX-3-Ni was degased at 75 ℃ for 15 h under dynamic pressure below 5μm Hg. C_2H_2 and C_2H_4 sorption isotherms were collected at 273~313 K on activated SIFSIX-1-Cu, SIFSIX-2-Cu, SIDSIX-2-Cu-i, and SIFSIX-3-Zn using ASAP 2050 Analyzer (Micromeritics), and SIFSIX-3-Ni and SIFSIX-3-Cu were conducted using 3Flex (Micromeritics).

Breakthrough tests

The breakthrough experiments were carried out in a dynamic gas breakthrough equipment (fig. S32). All experiments were conducted using a stainless steel column (4.6 mm inner diameter × 50 mm). According to the different particle size and density of the sample powder, the weight packed in the column was: 0.22 g SIFSIX-1-Cu powder, SIFSIX-2-Cu-i (column 1: 0.19 g, column 2: 0.21 g), and SIFSIX-3-Zn (column 1: 0.78 g, column 2: 0.70 g), respectively. The column packed with sample was firstly purged with He flow (15 ml min^{-1}) for 12 h at room temperature (25 ℃). The mixed gas (C_2H_2/C_2H_4: 50/50, v/v) flow was then introduced at 1.25 ml min^{-1}. Outlet gas from the column was monitored using gas chromatography (GC-8A or GC-2010 plus, SHIMADZU) with a flame ionization detector (FID). The standard gases were used to calibrate the concentration of the outlet gas. After the breakthrough experiment, the sample was regenerated with He flow (7 to 15 ml min^{-1}) for 6 to 20 hours. Then, the breakthrough tests of mixed gas (C_2H_2/C_2H_4: 1/99, v/v) were conducted on the packed bed of SIFSIX-1-Cu, SIFSIX-2-Cu-i and SIFSIX-3-Zn at 25 ℃.

A GC-2010 plus (SHIMADZU) was used for the measurement of C_2H_2 levels. The gas mixture was separated by a capillary column (Agilent GS-GASPRO, Φ0.32 × 60 M) at 323 K with a He flow rate of 2 ml/min. A standard gas mixture containg 40 ppm C_2H_2 was used to calibrate the concentration of C_2H_2.

In the processes of production of high-purity C_2H_4, the feed gases for the unit of C_2H_2 removal are contaminated with trace CO_2 (< 50 ppm), H_2O (< 5 ppm), and O_2 (< 5 ppm) (*28*). Therefore, the effect of CO_2, H_2O, and O_2 on the separation of C_2H_2 and C_2H_4 were investigated in this work.

Beakthrough tests of mixed gas ($C_2H_2/C_2H_4/CO_2$ or $C_2H_2/C_2H_4/O_2$). 0.21 g SIFSIX-1-Cu-i was packed in the column (4.6 mm inner diameter × 50 mm). After activation, the mixed gas flow was introduced at 1.25 ml min^{-1}. Outlet gas from the column was monitored using gas chromatography (GC-2010 plus) with a thermal conductivity detector (TCD) coupled with a FID. The gas mixture was separated by a capillary column (Agilent GS-GASPRO, Φ0.32 × 60 M) at 373 K with a He flow rate of 8 ml/min. The concentration of CO_2 or O_2 in the outlet gas was monitored by a TCD and the concentration of C_2H_2 and C_2H_4 were detected by a FID.

Beakthrough tests of mixed gas ($C_2H_2/C_2H_4/H_2O$). 0.21 g SIFSIX-1-Cu-i was packed in the column (4.6 mm inner diameter × 50 mm). The mixed gas flow was introduced at 1.25 ml min^{-1}. Outlet gas from the column was monitored using two gas chromatography in a series. The first gas chromatography is a GC-2010 plus with a TCD and a capillary column (Agilent HP-PLOT/Q, Φ0.53 × 30 M). The second gas chromatography is a GC-8A with a FID and a packed column (No. 15092203, JieDao Tech). The concentration of H_2O in the outlet gas was monitored by a TCD (GC-2010 plus) and the concentration of C_2H_2 and C_2H_4 were detected by a FID (GC-8A).

X-ray diffraction structure analysis

Powder X-Ray diffraction patterns were collected using SHIMADZU XRD-6000 diffractometer (Cu K_α λ = 1.540598 Å) with an operating power of 40 Kv and fixed divergence slit of 0.76 mm. The data were collected in the range of 2θ = 3-50 °.

Neutron diffraction 3xperiment

Neutron diffraction data were collected using the BT-1 neutron powder diffractometer at the National Institute of Standards and Technology (NIST) Center for Neutron Research. A Ge(311) monochromator with a 75 °take-off angle, λ = 2.0787(2) Å, and in-pile collimation of 60 minutes of arc was used. Data were collected over the range of 1.3-166.3 ° (2θ) with a step size of 0.05 °. Fully activated SIFSIX-1-Cu sample was loaded in a vanadium can equipped with a capillary gas line and a packless valve. A closed-cycle He refrigerator was used for sample temperature control. The bare MOF sample was measured first at the temperatures of 6 K, 100 K, 200 K, and 300 K. To probe the acetylene adsorption locations, a pre-determined amount of C_2D_2 (~4 C_2D_2 per SIFSIX-1-Cu and ~1.7C_2D_2 per SIFSIX-2-Cu-i; note that deuterated acetylene was used because H has large incoherent neutron scattering cross section, and thus would introduce large background in the diffraction data.) was loaded into the sample at room temperature, and the sample was slowly cooled to 200 K (at which point, nearly all gas molecules were adsorbed into the sample). Diffraction data were then collected on the C_2D_2-loaded MOF samples.

Rietveld structural refinement was performed on the neutron diffraction data using the GSAS package. (*29*) Refinement on lattice parameters, atomic coordinates, thermal factors, gas molecule occupancies, background, and profiles all converge with satisfactory R-factors.

Density-functional theory calculations

Neutro First-principles density-functional theory (DFT) calculations were performed using the Quantum-Espresso package. A semi-empirical addition of dispersive forces to conventional DFT was included in the calculation to account for van der Waals interactions. (*30*) We used Vanderbilt-type ultrasoft pseudopotentials and generalized gradient approximation (GGA) with Perdew-Burke-Ernzerhof (PBE) exchange correlation. A cutoff energy of 544 Ev and a 2 ×2 ×4 k-point mesh (generated using the Monkhosrt-Pack scheme) were found to be enough for the total energy to converge within 0.01 meV/atom. We first optimized the structure of SIFSIX MOFs. The optimized structures are good matches for the experimentally determined crystal structures of the coordination networks. Various guest gas molecules were then introduced to to various locations of the channel pore, followed by a full structural relaxation. To obtain the gas binding energy, an isolated gas molecule placed in a supercell (with the same cell dimensions as the MOF crystal) was also relaxed as a reference. The static binding energy (at T = 0 K) was then calculated using: EB = E(MOF) + E(gas) – E(MOF+gas).

Fitting of pure component isotherms

The DFT-D calculation and neutron powder diffraction experiments indicate that each F site in some SIFSIX materials can accommodate one gas molecules, which is in accord with the principal implicit assumptions of Langmuir isotherm model (*31*). However, strong interactions ($H^{\delta+}$•••$C^{\delta-}$ dipole-dipole) between neighboring adsorbates is observed in SIFSIX-1-Cu, which go against the another implicit assumption of Langmuir isotherm model (no interaction between neighboring adsorbates). In addition, in the case of SIFSIX-2-Cu-i, each gas molecule occupies two sites and the surface of materials is energetically uniform. In these cases, dual-Langmuir-Freundlich isotherm model (*31*) is reasonable selection for the correction of adsorption data.

The pure component isotherm data for C_2H_2 and C_2H_4 in SIFSIX-1-Cu, SIFSIX-2-Cu, SIFSIX-2-Cu-i, SIFSIX-3-Zn, SIFSIX-3-Ni, and SIFSIX-3-Cu were fitted with either the dual-Langmuir-Frendlich isotherm model.

$$q = q_{A,sat}\frac{b_A p^{\nu_A}}{1+b_A p^{\nu_A}} + q_{B,sat}\frac{b_B p^{\nu_B}}{1+b_B p^{\nu_B}} \quad (1)$$

or the single-site Langmuir-Freundlich model

$$q = q_{A,sat}\frac{b_A p^{\nu_A}}{1+b_A p^{\nu_A}} \quad (2)$$

with T-dependent parameters b_A, and b_B

$$b_A = b_{A0}\exp\left(\frac{E_A}{RT}\right); \quad b_B = b_{B0}\exp\left(\frac{E_B}{RT}\right) \quad (3)$$

The fitted parameter values are presented in Table 2, Table 3, Table 4, Table 5, Table 6 and Table 7. For all other MOFs, the isotherm data are taken from He *et al*. (*32*) and Hu *et al*. (*17*)

Isosteric heat of adsorption

The binding energy of C_2H_2 is reflected in the isosteric heat of adsorption, Qst, defined as

$$Q_{st} = RT^2\left(\frac{\partial \ln p}{\partial T}\right)_q \quad (4)$$

Fig. S19 presents a comparison of the heats of adsorption of C_2H_2 in various MOFs; the calculations are based on the use of the Clausius-Clapeyron equation.

IAST claculations of adsorption selectivities

The adsorption selectivity for C_2H_2/C_2H_4 separation is defined by

$$S_{ads} = \frac{q_1/q_2}{p_1/p_2} \quad (5)$$

q_1, and q_2 are the molar loadings in the adsorbed phase in equilibrium with the bulk gas phase with partial pressures p_1, and p_2.

Transient breakthrough of C_2H_2/C_2H_4 mixtures in fixed bed adsorbers

The performance of industrial fixed bed adsorbers is dictated by a combination of adsorption selectivity and uptake capacity. For a proper comparison of various MOFs, we perform transient breakthrough simulations using the simulation methodology described in the literature. (*27, 33*) For the breakthrough simulations, the following parameter values were used: length of packed bed, L = 0.12 m; voidage of packed bed, ε = 0.75; superficial gas velocity at inlet, u = 0.003 m/s. The transient breakthrough simulation results are presented in terms of a dimensionless time, τ, defined by dividing the actual time, t, by the characteristic time, $\frac{L\varepsilon}{u}$.

We investigated the separation performance of SIFSIX materials, SIFSIX MOFs, FeMOF-74, NOTT-300, UTSA-100a, and M'MOF-3a for separation of 1/99 and 50/50 C_2H_2/C_2H_4 feed mixtures. The total bulk gas phase is at 298 K and 100 kPa. The amount of adsorbed C_2H_2 during the time interval 0-τ_{break} (τ_{break} is the dimensionless breakthrough times) was calculated according to the materials balance and the values are presented in Fig. 3, C and F as a function of τ_{break}.

Table S1 to S15

Table S1. Summary of the adsorption uptakes, selectivities and heat of adsorption data for C_2H_2 and C_2H_4 in various MOFs.

	Surface area (m^2/g, BET)	Pore size (Å)	C_2H_2 uptake at 1.0 bar (mmol/g)	C_2H_4 uptake at 1.0 bar (mmol/g)	Selectivity for C_2H_2/C_2H_4 at 1/99 mixture†	Selectivity for C_2H_2/C_2H_4 at 50/50 mixture†	Q_{st} (C_2H_2, KJ/mol)§	ΔE (C_2H_2, KJ/mol)	Q_{st} (C_2H_4, KJ/mol)§	ΔE (C_2H_4, KJ/mol)
M'MOF-3a (*19*)	110	3.4×4.8	1.9*	0.4*	24.03	34.17	25	-	-	-
UTSA-100a (*17*)	970	4.3×4.3	4.27*	1.66*	10.72	19.55	22	-	-	-
NOTT-300 (*14*)	1370	6.5×6.5	6.34‡	4.28‡	2.17	2.3	32	-	-	-
FeMOF-74 (*18*)	1350	11×11	6.8#	6.1#	2.08	2.1	46	-	-	-
SIFSIX-3-Zn	250	4.2×4.2	3.64	2.24	8.82	13.72	21/31&	50.3	28.8	47.4
SIFSIX-3-Ni	368	4.2×4.2	3.30	1.75	5.03	5.98	30.5	-	30.3	-
SIFSIX-2-Cu-i	503	5.2×5.2	4.02	2.19	44.54	41.01	41.9	52.9	30.7	39.8
SIFSIX-2-Cu	1881	10.5×10.5	5.38	2.02	6.0	4.95	26.3	34.6	20.8	-
SIFSIX-1-Cu	1178	8.0×8.0	8.50	4.11	10.63	8.37	30/37&	44.6/47.0$	23.5	27.2

Summary of the adsorption data were collected at 298 K

* At temperature of 296 K;

‡ At temperature of 293 K;

At temperature of 318 K;

† IAST selectivity;

§ Q_{st} values at low surface coverage;

& Highest Q_{st} values at different surface coverage.

$ Δ*E* of SIFSIX-1-Cu•1C_2H_2 (44.6 kJ/mol) and SIFSIX-1-Cu•4C_2H_2 (47 kJ/mol)

Table S2. Langmuir-Freundlich parameter fits for C_2H_2 and C_2H_4 in SIFSIX-1-Cu.

	Site A				Site B			
	$q_{A,sat}$ mol kg^{-1}	b_{A0} $Pa^{-\nu_i}$	E_A kJ mol^{-1}	ν_A dimensionless	$q_{B,sat}$ mol kg^{-1}	b_{B0} $Pa^{-\nu_i}$	E_B kJ mol^{-1}	ν_B dimensionless
C_2H_2	3.1	2.3×10^{-24}	90	2	6.2	5.87×10^{-10}	29	1
C_2H_4	16.6	3.22×10^{-11}	25.8	1.1				

Table S3. Langmuir-Freundlich parameter fits for C_2H_2 and C_2H_4 in SIFSIX-2-Cu.

	$q_{A,sat}$ mol kg^{-1}	b_{A0} $Pa^{-\nu_i}$	E_A kJ mol^{-1}	ν_A dimensionless
C_2H_2	17.8	8.93×10^{-9}	21	0.8
C_2H_4	13.3	3.96×10^{-10}	20.8	1

Table S4. Langmuir-Freundlich parameter fits for C_2H_2 and C_2H_4 in SIFSIX-3-Zn. Note that the isotherms for C_2H_4 were measured only at 298 K; consequently, the energy parameter is not reported for C_2H_4.

	Site A				Site B			
	$q_{A,sat}$ mol kg^{-1}	b_{A0} $Pa^{-\nu_i}$	E_A kJ mol^{-1}	ν_A dimensionless	$q_{B,sat}$ mol kg^{-1}	b_{B0} $Pa^{-\nu_i}$	E_B kJ mol^{-1}	ν_B dimensionless
C_2H_2	2.6	5.43×10^{-10}	30	0.95	1.6	1.76×10^{-10}	27	1.57
C_2H_4	2.45	5.09×10^{-6}		1.26				

Table S5. Langmuir-Freundlich parameter fits for C_2H_2 and C_2H_4 in SIFSIX-2-Cu-i.

	Site A				Site B			
	$q_{A,sat}$ mol kg^{-1}	b_{A0} $Pa^{-\nu_i}$	E_A kJ mol^{-1}	ν_A dimensionless	$q_{B,sat}$ mol kg^{-1}	b_{B0} $Pa^{-\nu_i}$	E_B kJ mol^{-1}	ν_B dimensionless
C_2H_2	2.2	1.08×10^{-11}	37.5	1	2.3	7.94×10^{-11}	42	1
C_2H_4	3.5	7.23×10^{-11}	30.7	1				

Table S6. Langmuir-Freundlich parameter fits for C_2H_2 and C_2H_4 in SIFSIX-3-Ni.

	Site A				Site B			
	$q_{A,sat}$ mol kg^{-1}	b_{A0} $Pa^{-\nu_i}$	E_A kJ mol^{-1}	ν_A dimensionless	$q_{B,sat}$ mol kg^{-1}	b_{B0} $Pa^{-\nu_i}$	E_B kJ mol^{-1}	ν_B dimensionless
C_2H_2	3	7.41×10^{-10}	30.7	1	1	1.92×10^{-9}	20.3	1
C_2H_4	3.3	4.42×10^{-12}	33.3	1.1				

Table S7. Langmuir-Freundlich parameter fits for C_2H_2 in SIFSIX-3-Cu.

	Site A				Site B			
	$q_{A,sat}$ mol kg^{-1}	b_{A0} $Pa^{-\nu_i}$	E_A kJ mol^{-1}	ν_A dimensionless	$q_{B,sat}$ mol kg^{-1}	b_{B0} $Pa^{-\nu_i}$	E_B kJ mol^{-1}	ν_B dimensionless
C_2H_2	1.9	1.62×10^{-9}	26.5	1	1.83	6.91×10^{-9}	31.1	1

Table S8. Breakthrough calculations for separation of C_2H_2/C_2H_4 mixture (1/99) at 298 K. The data for FeMOF-74 is at a temperature of 318 K; this is the lowest temperature used in the isotherm measurements of Bloch *et al*. (*18*). The data for NOTT-300 is at 293 K, for which the isotherm data is available in Yang *et al.* (*14*). The product gas stream contains less than 40 ppm C_2H_2.

	Dimensionless breakthrough time τ_{break}	C_2H_2 adsorbed during 0 - τ_{break} mmol L^{-1}
SIFSIX-1-Cu	219.83	265.33
SIFSIX-2-Cu	43.87	52.33
SIFSIX-3-Zn	175.16	211.00
SIFSIX-2-Cu-i	644.90	780.00
SIFSIX-3-Ni	103.73	124.67
FeMOF-74	89.40	100.67
M'MOF3a	58.45	69.67
UTSA-100a	56.28	135.33
NOTT-300	112.39	68.33

Table S9. Breakthrough calculations for separation of C_2H_2/C_2H_4 mixture (50/50) at 298 K. The data for FeMOF-74 is at a temperature of 318 K; this is the lowest temperature used in the isotherm measurements of Bloch *et al*. (*18*). The data for NOTT-300 is at 293 K, for which the isotherm data is available in Yang *et al.* (*14*). The product gas stream contains less than 40 ppm C_2H_2.

	Dimensionless breakthrough time τ_{break}	C_2H_2 adsorbed during 0 - τ_{break} mmol L^{-1}
SIFSIX-1-Cu	92.31	5533
SIFSIX-2-Cu	30.57	1797
SIFSIX-3-Zn	74.14	4433
SIFSIX-2-Cu-i	67.69	4033
SIFSIX-3-Ni	58.38	3467
FeMOF-74	71.52	4000
M'MOF3a	21.70	1257
UTSA-100a	52.04	3153
NOTT-300	56.14	3333

Table S10. List of atomic positions for SIFSIX-1-Cu•C_2D_2

Atom	a	b	c	U (Å^2)
C1	-0.0364(4)	0.24630(28)	0.31708(23)	0.0232
C2	-0.0355(4)	0.37130(28)	0.32101(24)	0.0232
H3	-0.0632(9)	0.1915(9)	0.3699(5)	0.0435
H4	-0.0688(10)	0.4143(8)	0.3771(4)	0.0435
F5	0.1091(9)	0.1060(8)	1/2	0.0328
C6	0	0.4339(5)	1/4	0.0192
N7	0	0.1821(4)	1/4	0.0072
Cu8	0	0	1/4	0.0175
Si9	0	0	0.5	0.0147
F10	0	0	0.3917(5)	0.0076
C11	0.1907(4)	0.3693(7)	1/2	0.1066
C12	0.2396(4)	0.4660(7)	1/2	0.1066
D13	0.1492(4)	0.2874(7)	1/2	0.1359
D14	0.2811(4)	0.5479(7)	1/2	0.1359

Unit cell parameters	
Formula sum	C27.91 H16 D7.91 Cu F6 N4 Si
Formula weight	628.98 g/mol
Crystal system	tetragonal
Space-group	P 4/m c c (124)
Cell parameters	a=11.1037(3) Å c=15.9395(6) Å
Cell ratio	a/b=1.0000 b/c=0.6966 c/a=1.4355
Cell volume	1965.22(9) Å^3
Z	2
Calc. density	1.06287 g/cm^3

Table S11. List of atomic positions for SIFSIX-2-Cu-i•C_2D_2

Atom	a	b	c	U (Å^2)
C1	0.0227(4)	0.19917(25)	0.1404(4)	0.0140
C2	0.02506(28)	0.30028(25)	0.1469(4)	0.0140
H3	0.0353(10)	0.1575(9)	0.2551(10)	0.0535
H4	0.0366(9)	0.3363(10)	0.2674(10)	0.0535
C5	0	0.6479(4)	0	0.0297
C6	0	0.5447(4)	0	0.0297
N7	0	0.14897(34)	0	0.0240
Cu8	0	0	0	0.0281
Si9	0	0	1/2	0.0113
F10	0	0	0.2830(13)	0.0265
F11	0.0878(4)	0.0878(4)	1/2	0.0293
D	0.1901(8)	0.1901(8)	0.4012(17)	0.0964
C	0.2293(6)	0.2293(6)	0.3024(12)	0.0527

Unit cell parameters	
Formula sum	C27.38 H16 Cu D3.38 F6 N4 Si
Formula weight	613.43 g/mol
Crystal system	tetragonal
Space-group	I 4/m m m (139)
Cell parameters	a=13.7150(4) Å c=7.9523(3) Å
Cell ratio	a/b=1.0000 b/c=1.7247 c/a=0.5798
Cell volume	1495.83(7) Å^3
Z	2
Calc. density	1.36187 g/cm^3

Table S12. Comparison of the amount of C_2H_2 captured between experimental column breakthrough and simulated column breakthrough for C_2H_2/C_2H_4 separations (1/99) at 298 K.

	Experimental C_2H_2 uptake* mmol g^{-1}	C_2H_2 uptake from Simulation* mmol g^{-1}
SIFSIX-1-Cu	0.38	0.38
SIFSIX-2-Cu-i	0.73	0.70
SIFSIX-3-Zn	0.08	0.16

* The amount of C_2H_2 captured during the time interval 0 to 95% F/F^0. All experiments were conducted using a stainless steel column (4.6 mm inner diameter × 50 mm) at a flow rate of 1.25 ml/min.

Table S13. Comparison of the amount of C_2H_2 captured between experimental column breakthrough and simulated column breakthrough for C_2H_2/C_2H_4 separations (50/50) at 298 K.

	Experimental C_2H_2 uptake* mmol g^{-1}	C_2H_2 uptake from Simulation* mmol g^{-1}
SIFSIX-1-Cu	6.37	6.71
SIFSIX-2-Cu-i	2.88	3.27
SIFSIX-3-Zn	1.52	2.93

* The amount of C_2H_2 captured during the time interval 0 to 95% F/F^0. All experiments were conducted using a stainless steel column (4.6 mm inner diameter × 50 mm) at a flow rate of 1.25 ml/min.

Table S14. The volumetric uptake of C_2H_2 (density per crystal cell volume) in various SIFSIX materials at 1 bar.

	Framework density (g/cm^3)	C_2H_2 density per crystal cell volume (g/cm^3)		
		298 K	283 K	273 K
SIFSIX-1-Cu	0.864	0.191	0.206	-
SIFSIX-2-Cu	0.635	0.089	0.120	-
SIFSIX-2-Cu-i	1.247	0.131	0.142	-
SIFSIX-3-Zn	1.574	0.149	0.158	-
SIFSIX-3-Ni	1.610	0.138	-	0.150
SIFSIX-3-Cu	1.605	0.148	-	0.156

Table S15. The storage density of C_2H_2 in the pore of various SIFSIX materials at 1 bar.

	Pore volumes (cm^3/g)	C_2H_2 density per pore volume		
		298 K	283 K	273 K
SIFSIX-1-Cu	0.57	0.388	0.418	-
SIFSIX-2-Cu	1.10	0.127	0.172	-
SIFSIX-2-Cu-i	0.26	0.403	0.439	-
SIFSIX-3-Zn	0.19	0.499	0.518	-
SIFSIX-3-Ni	0.157	0.547	-	0.595
SIFSIX-3-Cu	0.158	0.583	-	0.615

Fig. S1 to S32

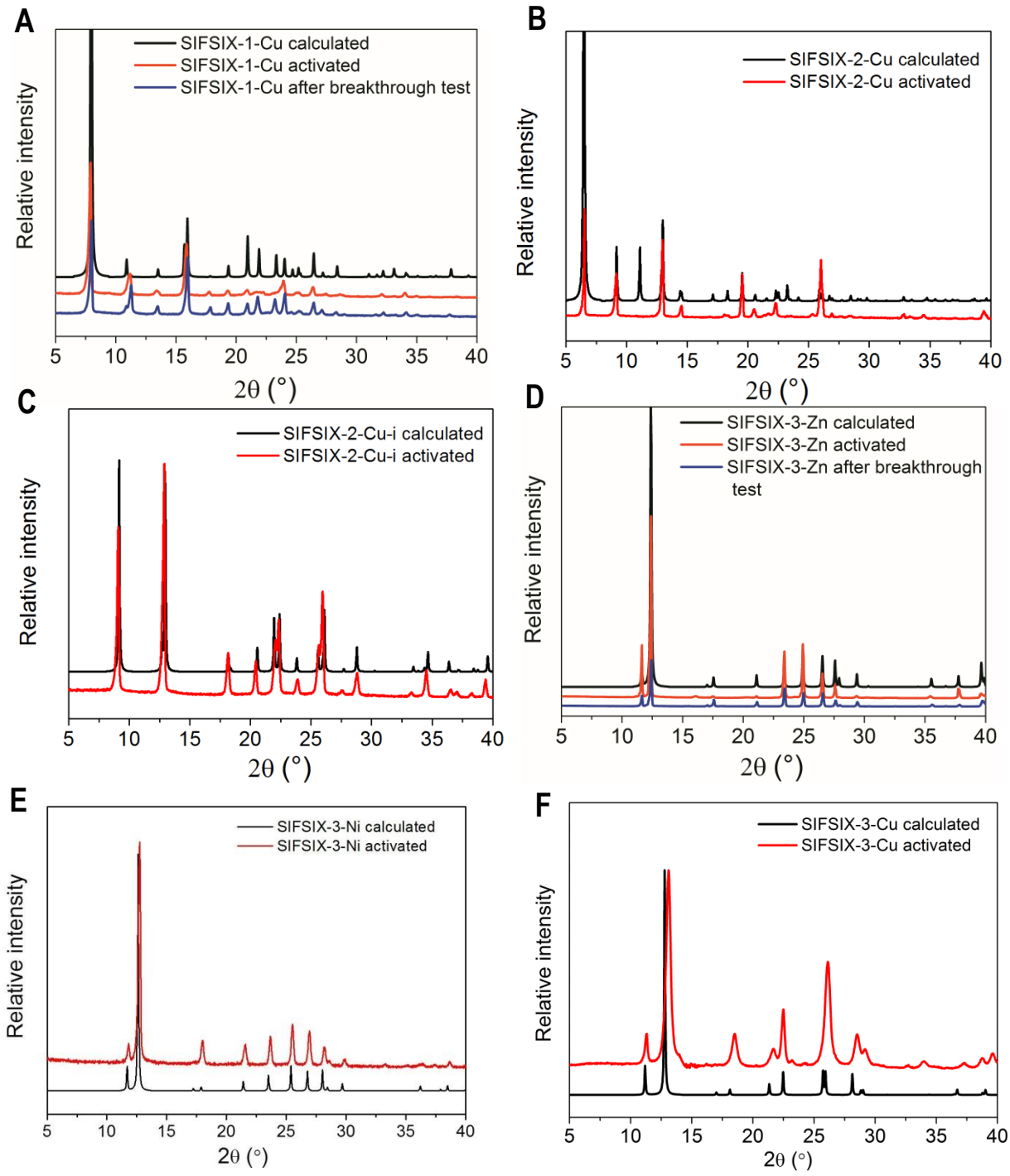

Fig. S1.
XRD patterns of sample SIFSIX-1-Cu (A), SIFSIX-2-Cu (B), SIFSIX-2-Cu-i (C), SIFSIX-3-Zn (D), SIFSIX-3-Ni (E) and SIFSIX-3-Cu (F).

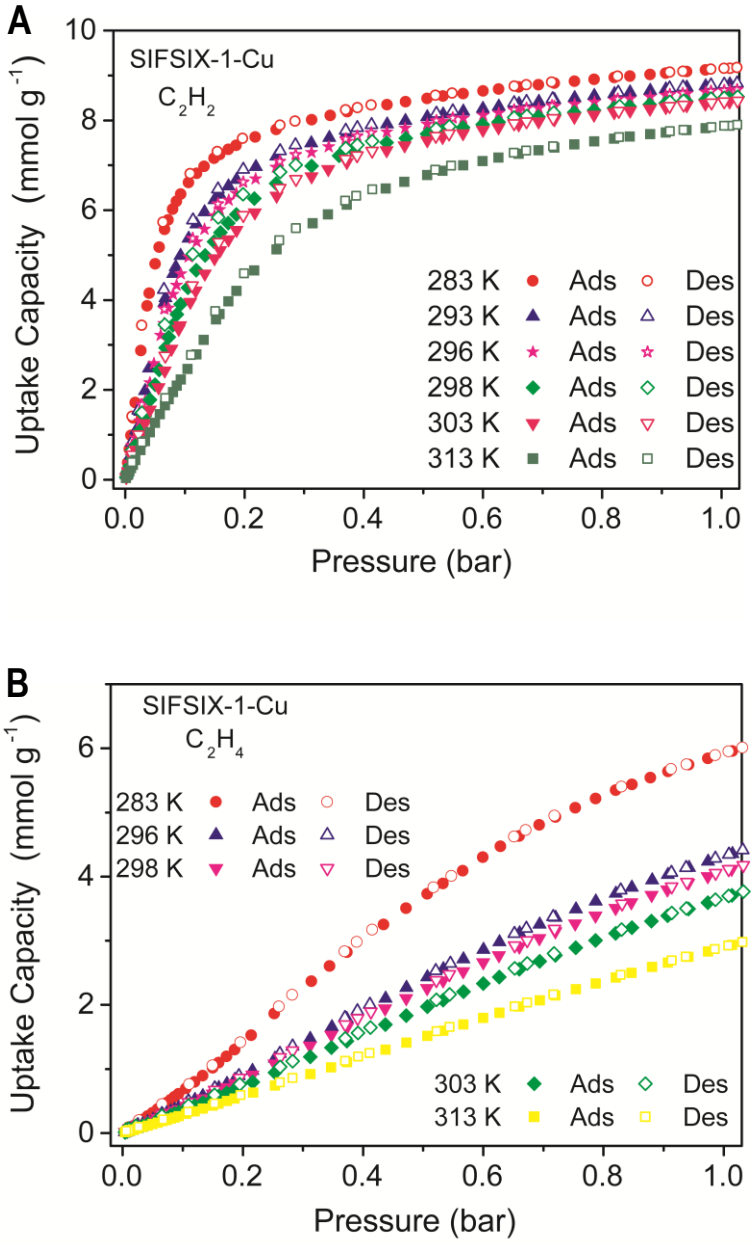

Fig. S2.
Adsorption isotherms for C_2H_2 (A) and C_2H_4 (B) on SIFSIX-1-Cu at different temperatures.

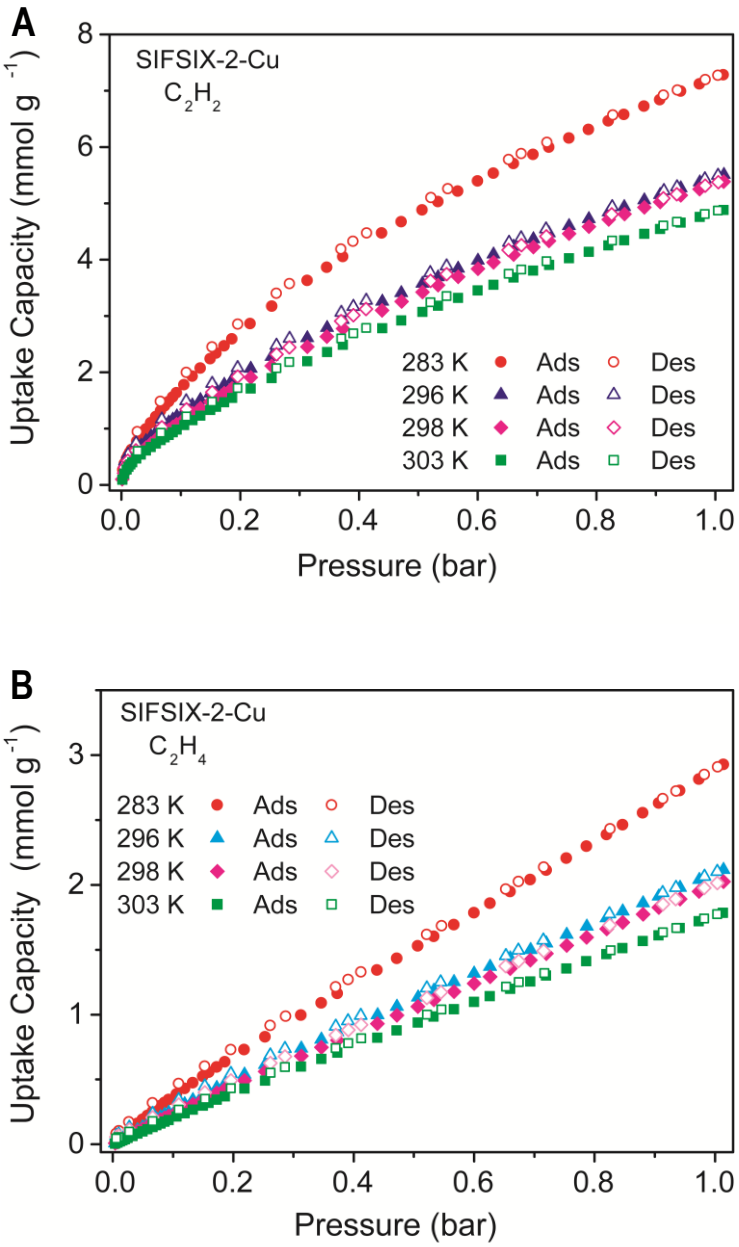

Fig. S3.
Adsorption isotherms for C_2H_2 (A) and C_2H_4 (B) on SIFSIX-2-Cu at different temperatures.

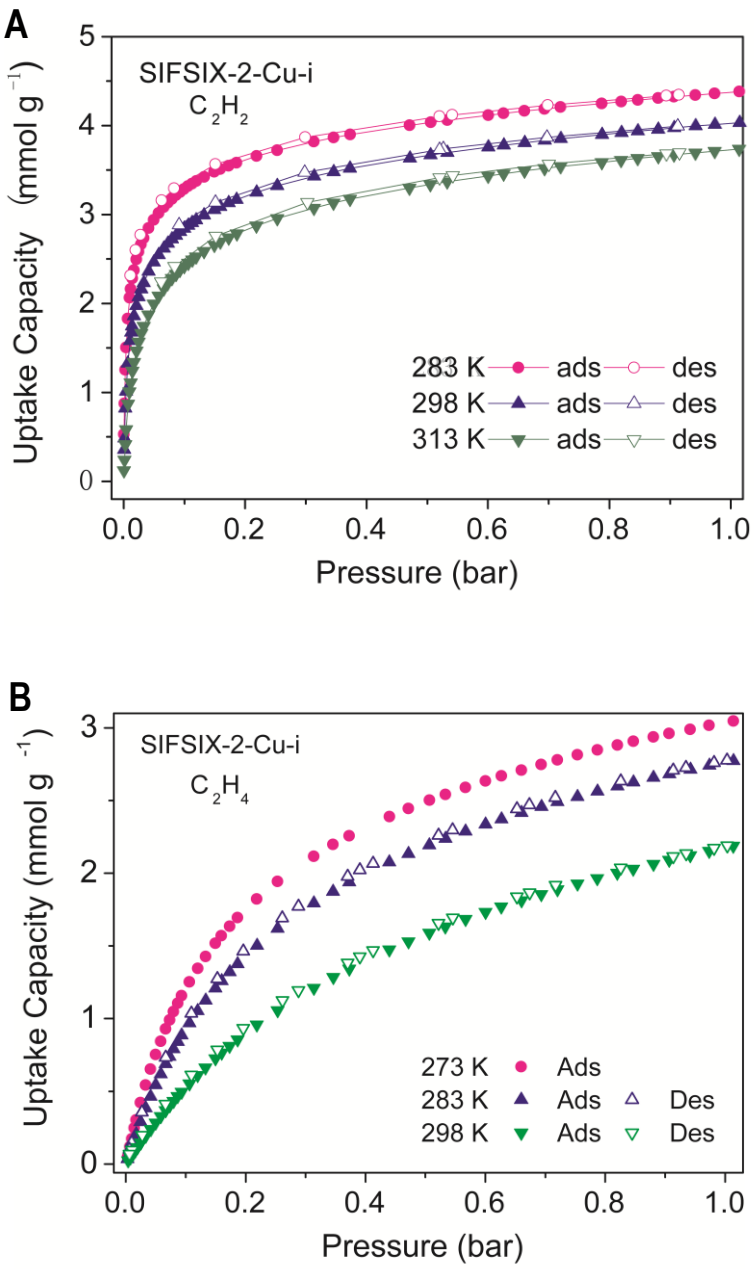

Fig. S4.
Adsorption isotherms for C_2H_2 (A) and C_2H_4 (B) on SIFSIX-2-Cu-i at different temperatures.

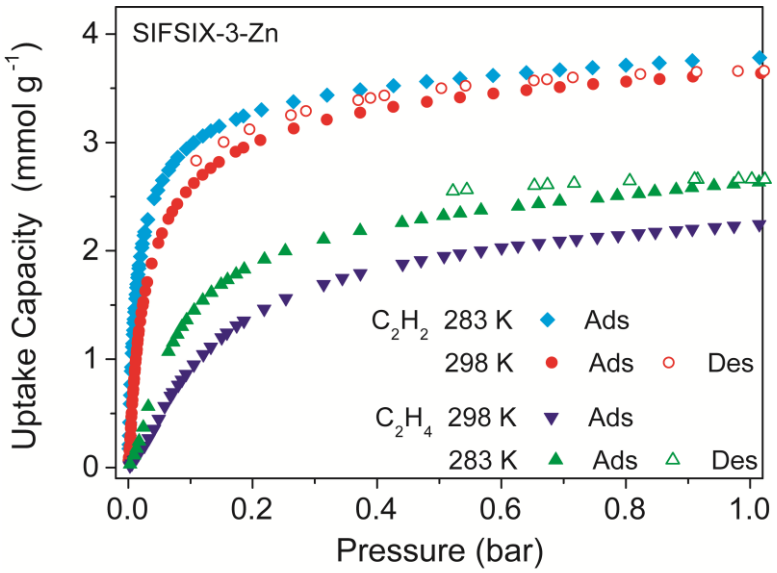

Fig. S5.
Adsorption isotherms for C_2H_2 and C_2H_4 on SIFSIX-3-Zn at different temperatures.

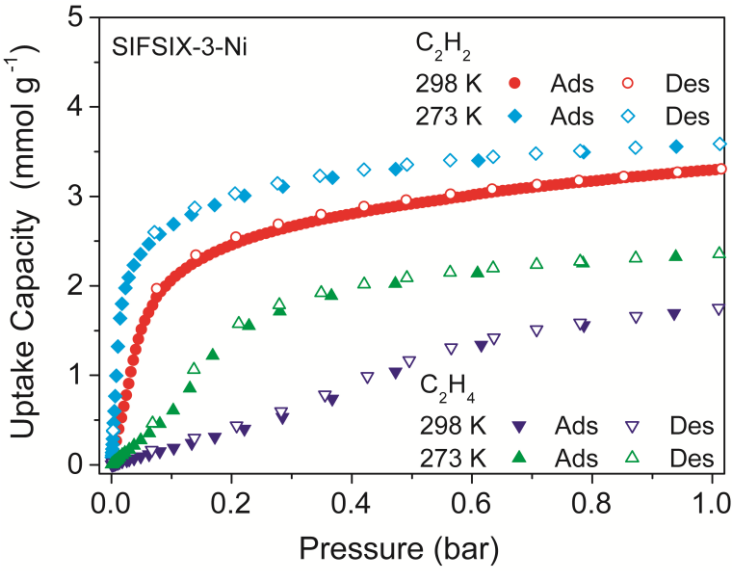

Fig. S6.
Adsorption isotherms for C_2H_2 and C_2H_4 on SIFSIX-3-Ni at different temperatures.

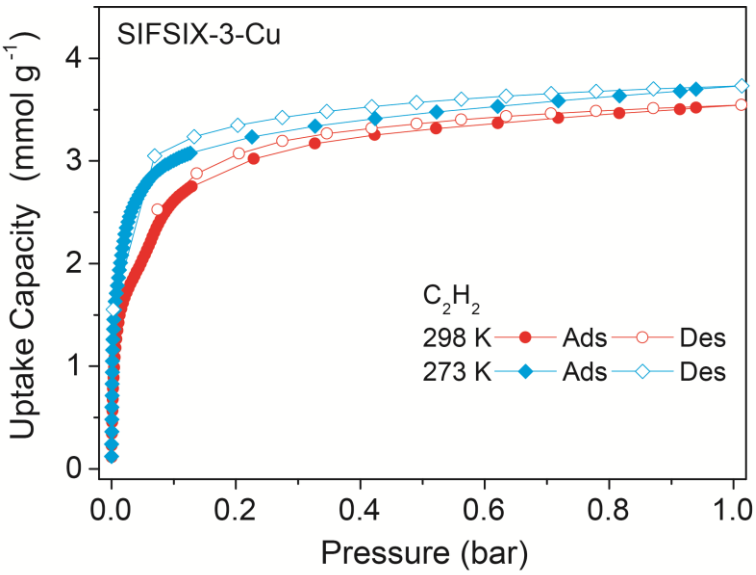

Fig. S7.
Adsorption isotherms of C_2H_2 on SIFSIX-3-Cu at 273 and 298 K.

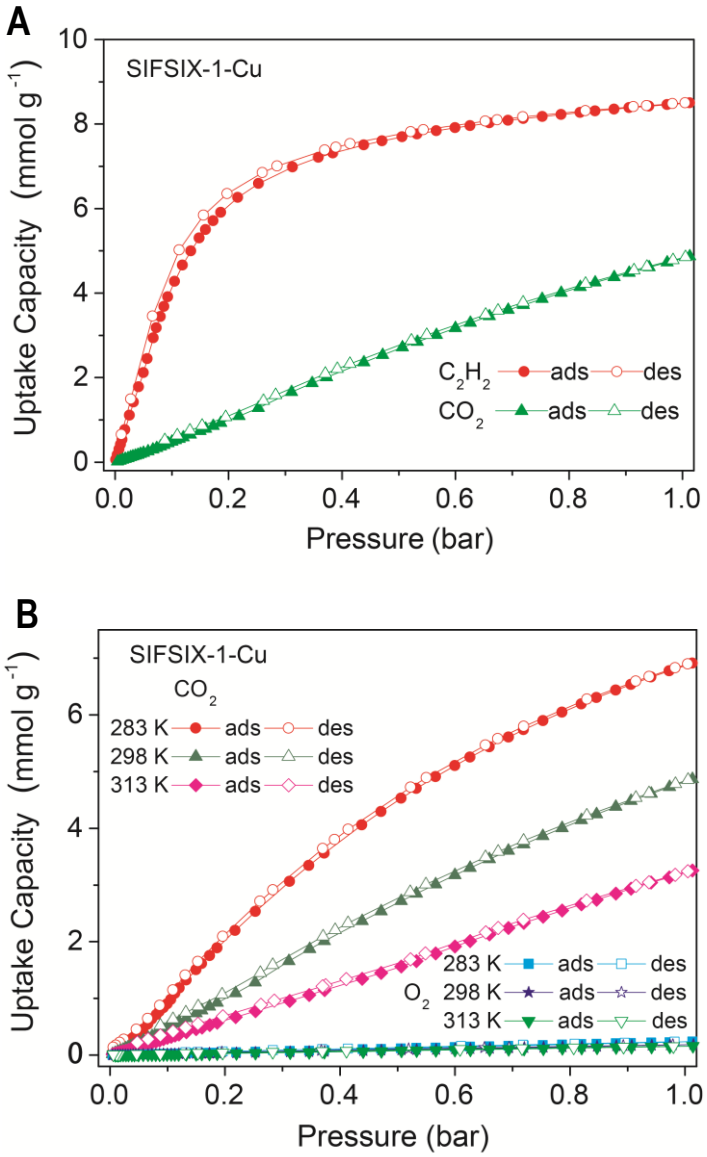

Fig. S8.
Comparison of C_2H_2 and CO_2 adsorption isotherms for SIFSIX-1-Cu at 298 K. (B) CO_2 and O_2 adsorption isotherms for SIFSIX-1-Cu at 283 K, 298 K and 313 K. Burd *et al.* previously reported adsorption data for CO_2 by SIFSIX-1-Cu (*34*).

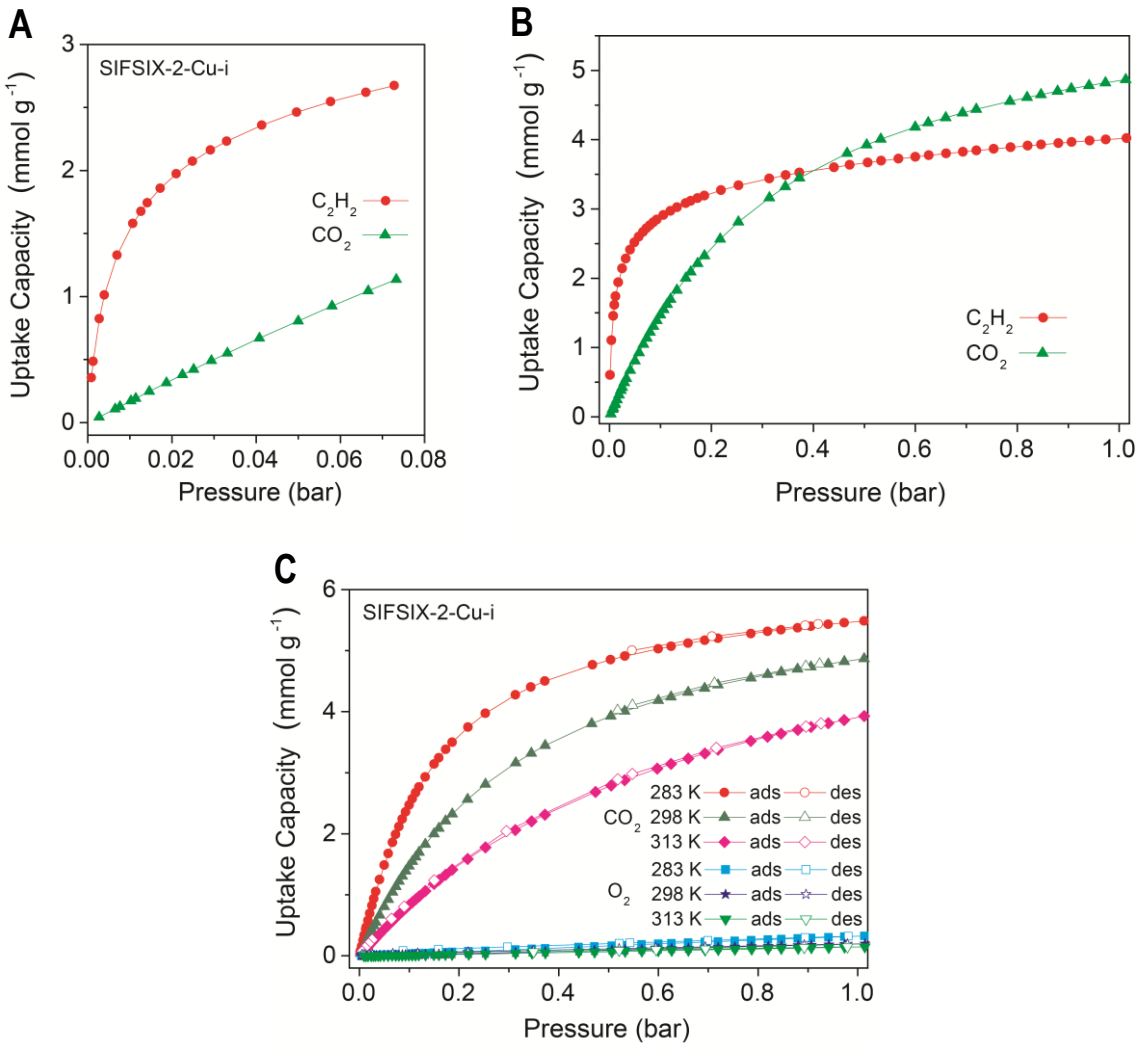

Fig. S9.
(A and B) Comparison of C_2H_2 and CO_2 adsorption isotherms for SIFSIX-2-Cu-i at 0-0.08 bar (**A**) and 0-1.0 bar (B) at 298 K. (C) CO_2 and O_2 adsorption isotherms for SIFSIX-2-Cu-i at 283 K, 2987 K and 313 K. Nugent et. al reported the adsorption data for CO_2 on SIFSIX-2-Cu-i (*20*).

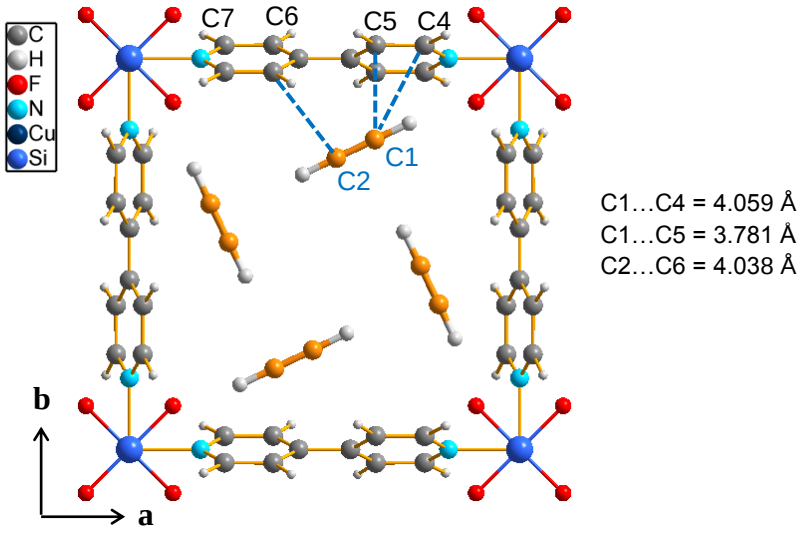

Fig. S10.
Schematic picture showing the DFT optimized C_2H_2 configuration in SIFSIX-1-Cu.

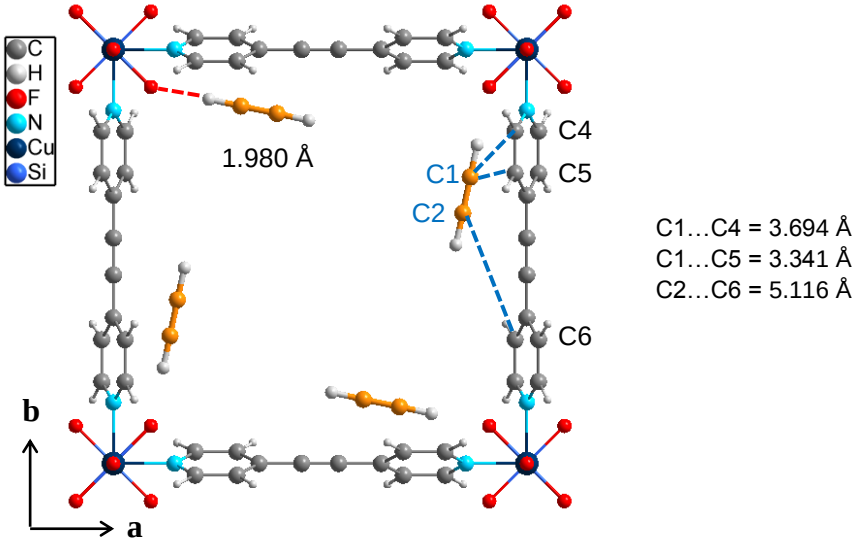

Fig. S11.
Schematic picture showing the DFT optimized C_2H_2 adsorption configuration in SIFSIX-2-Cu.

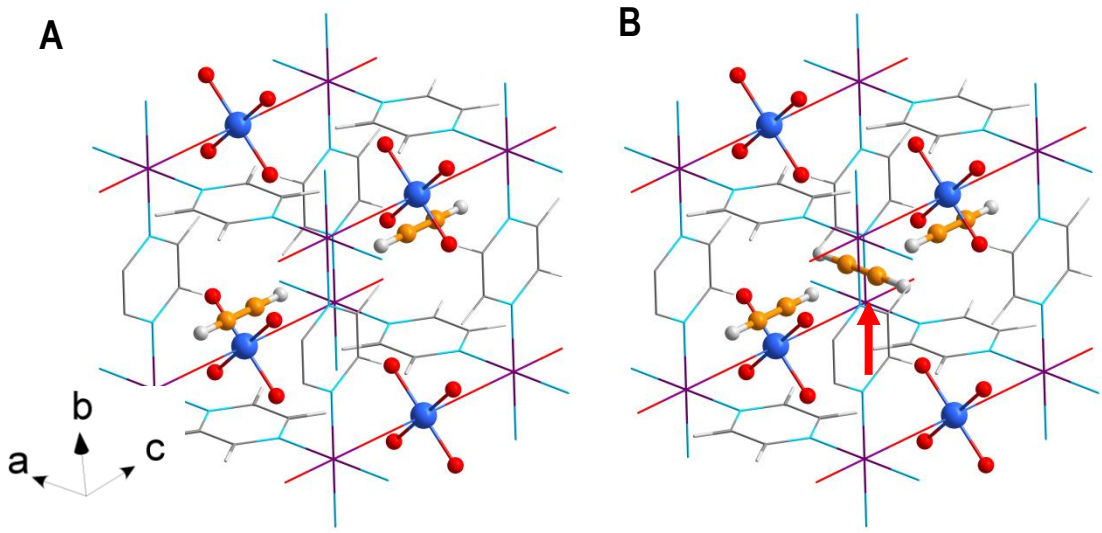

Fig. S12
Schematic pictures reveal the two the DFT optimized C_2H_2 adsorption binding sites in SIFSIX-3-Zn. The primary C_2H_2 adsorption site is shown on the left panel (A). A weaker secondary adsorption site is highlighted in the right panel (B).

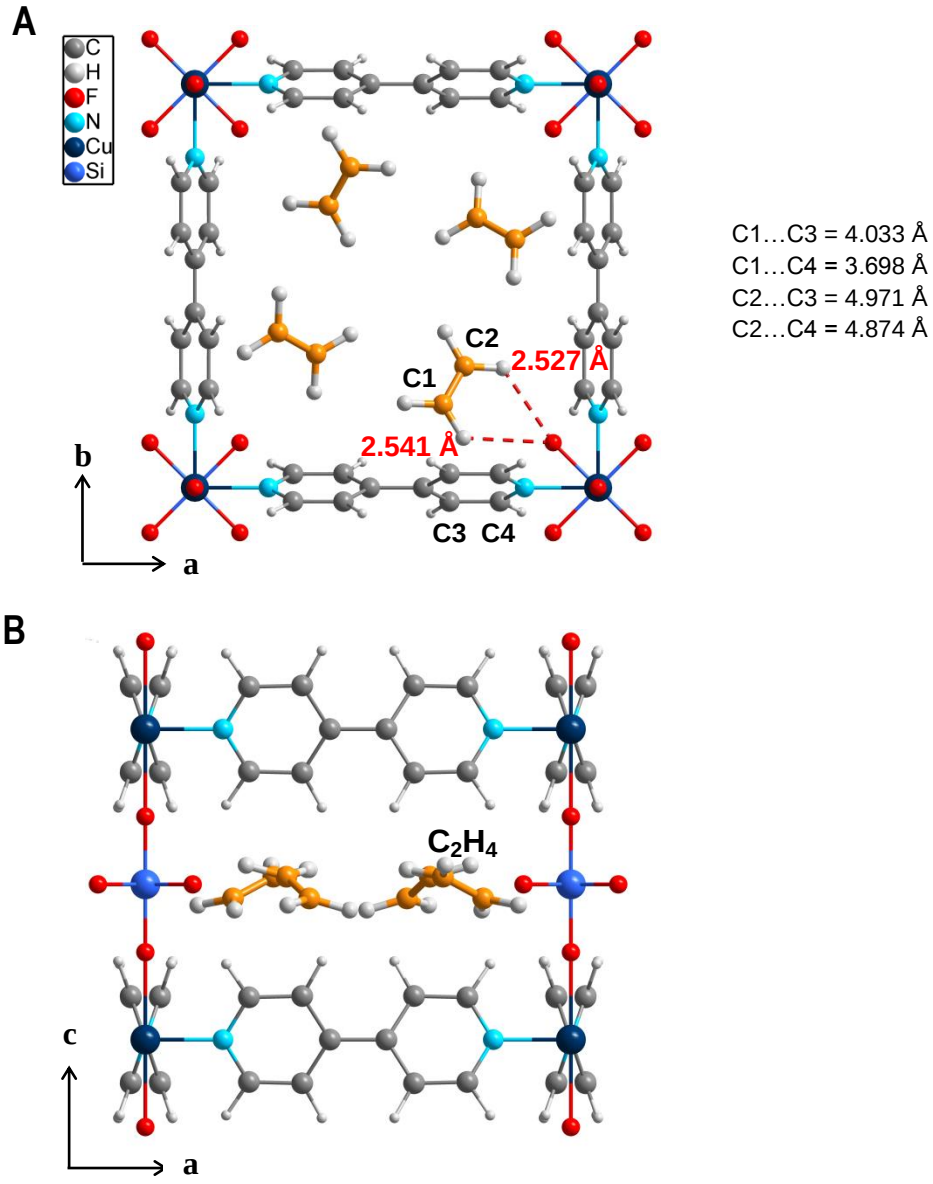

Fig. S13.
Schematic pictures showing the DFT optimized C_2H_4 adsorption configuration in SIFSIX-1-Cu.

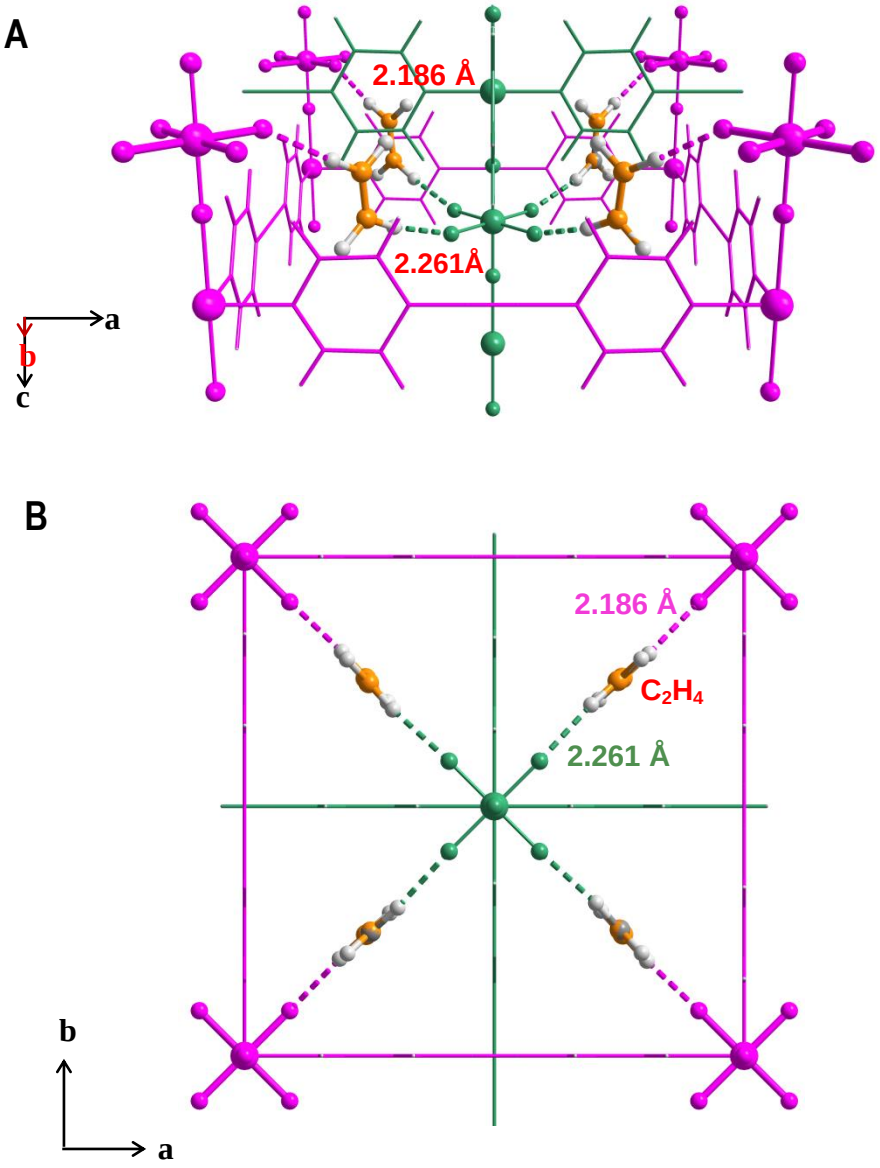

Fig. S14.
Schematic pictures showing the DFT optimized C_2H_4 adsorption configuration in SIFSIX-2-Cu-i.

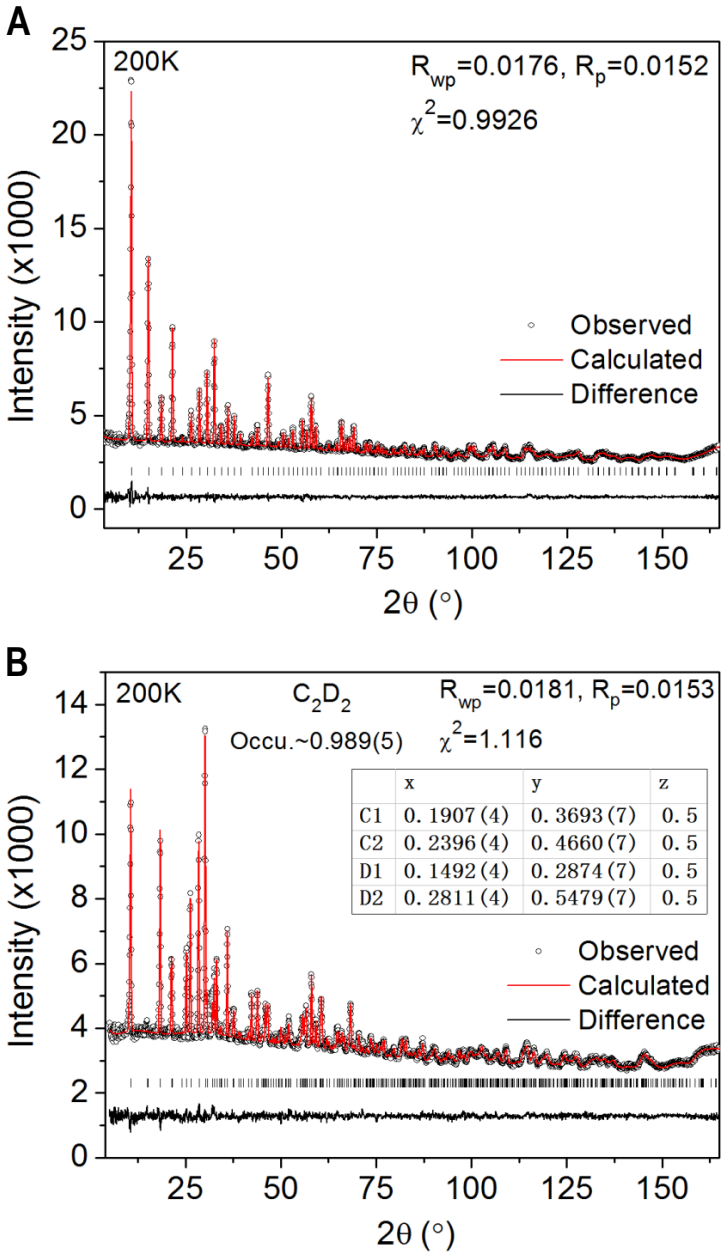

Fig. S15.
Neutron powder diffraction patterns for the Rietveld refinement of bare SIFSIX-1-Cu (A) and C_2D_2-loaded SIFSIX-1-Cu (B). Goodness of fit data: (A) R_{wp}=0.0176, R_p=0.0152, χ^2=0.9926; (B) R_{wp}=0.0181, R_p=0.0153, χ^2=1.116.

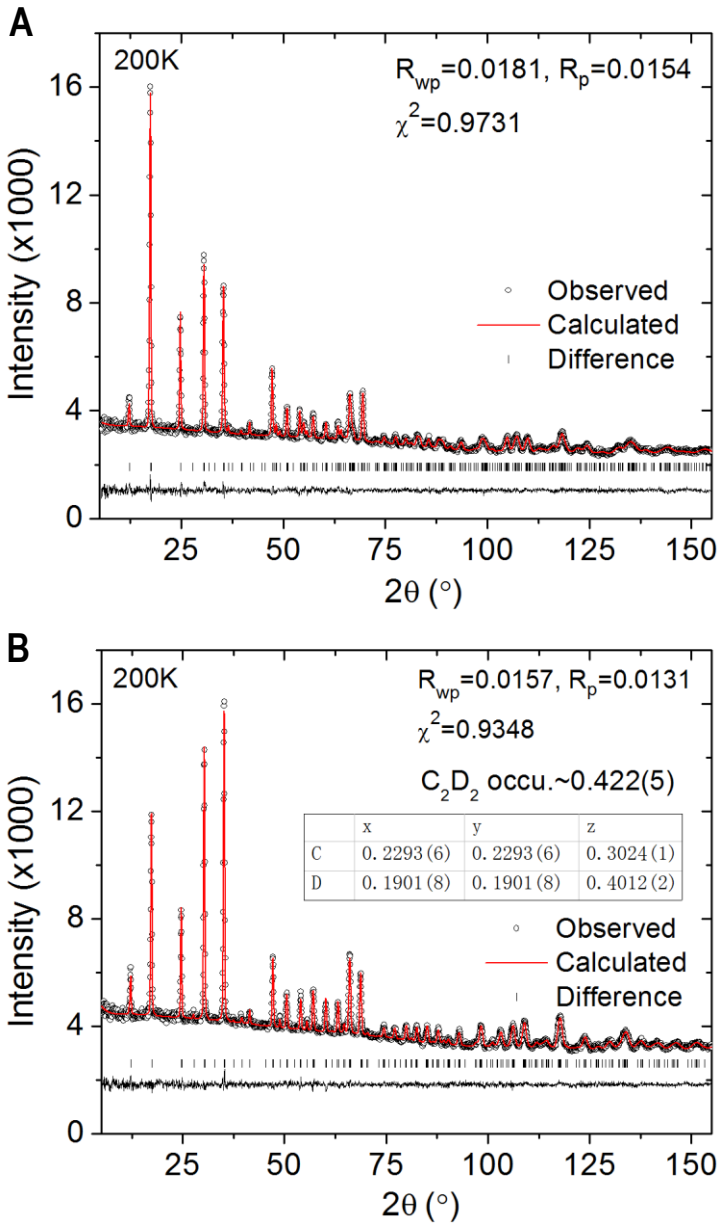

Fig. S16.
Neutron powder diffraction patterns for the Rietveld refinement of bare SIFSIX-2-Cu-i (A) and C_2D_2-loaded SIFSIX-2-Cu-i (B). Goodness of fit data: (A) R_{wp}=0.0181, R_p=0.0154, χ^2=0.9731; (B) R_{wp}=0.0157, R_p=0.0131, χ^2=0.9348.

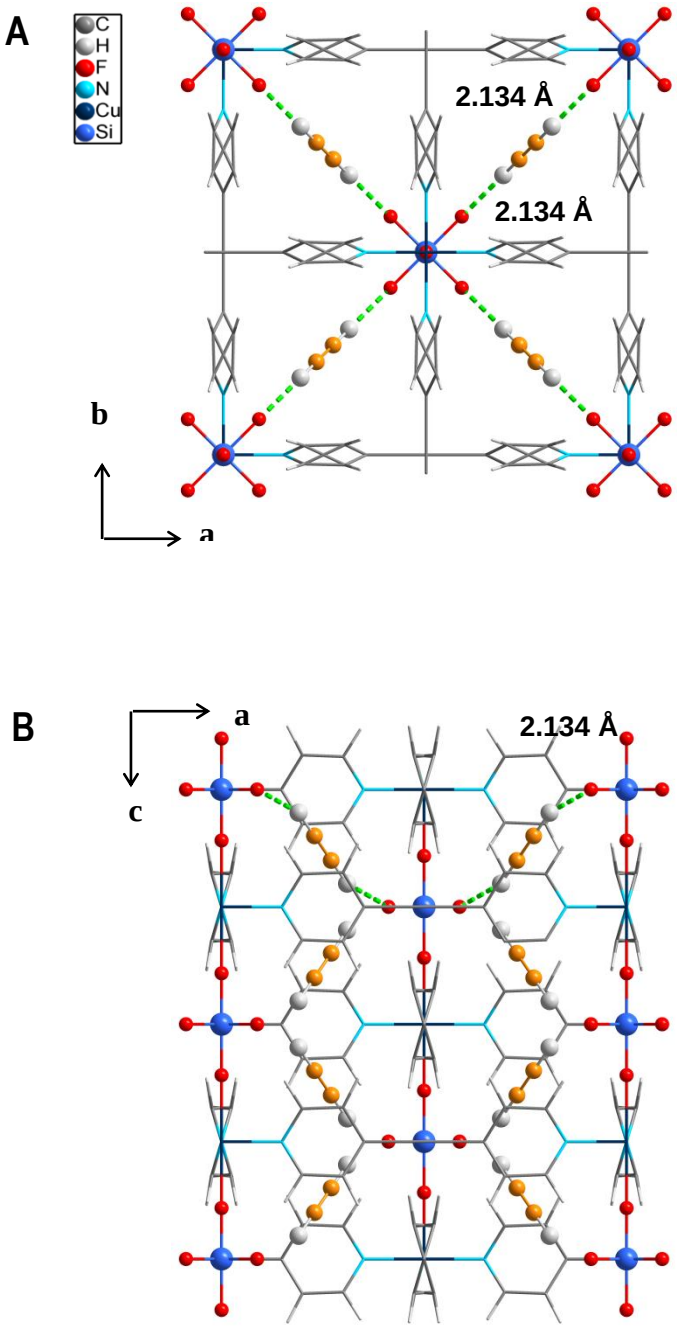

Fig. S17.
Neutron crystal structure of SIFSIX-2-Cu-i·1.7C_2D_2 at 200 K from Rietveld analysis. Perspective views down the *c* axis (A) and *b* axis (B) reveal the cooperative dual C-H•••F H-bonding interaction between C_2D_2 and SIFSIX-2-Cu-i.

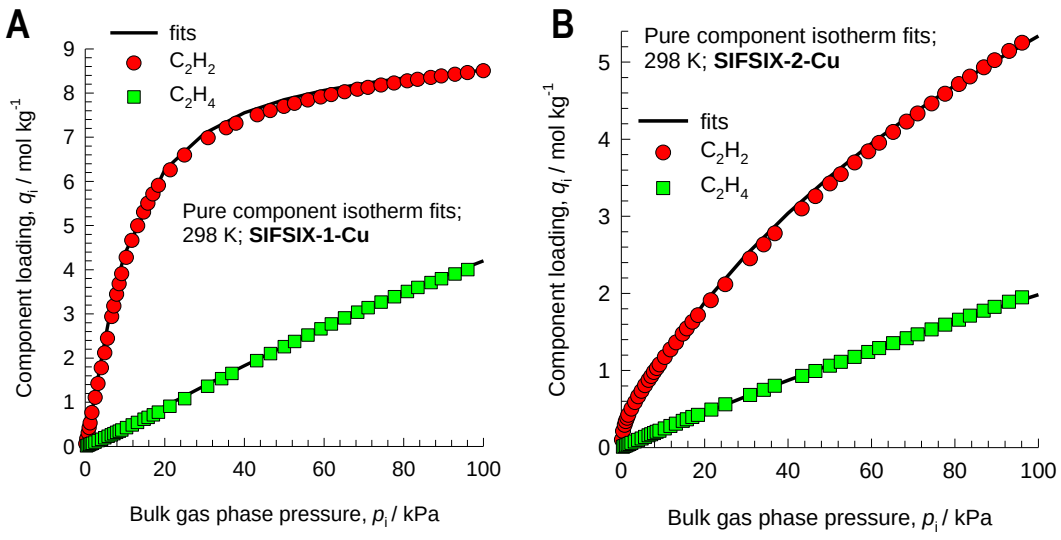

Fig.S18.
Comparison of component loadings for C_2H_2 and C_2H_4 at 298 K in SIFSIX-1-Cu (A), SIFSIX-2-Cu (B).

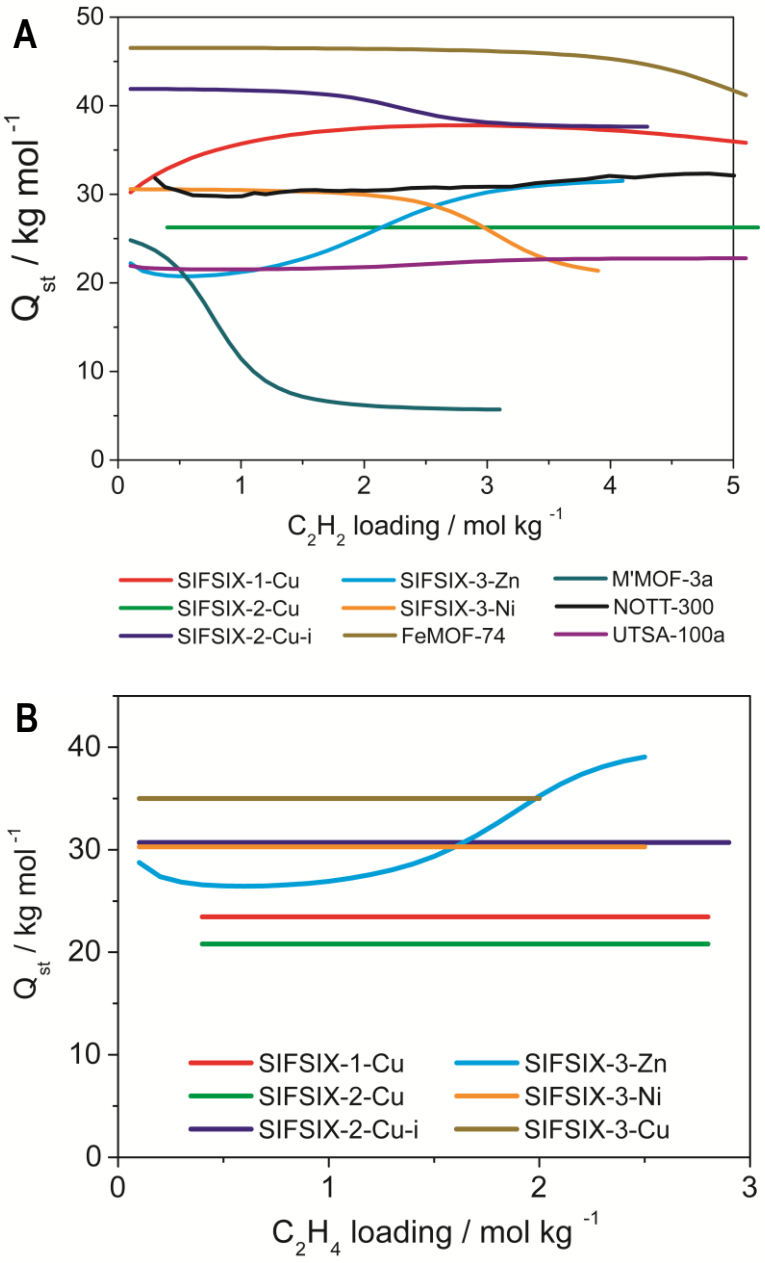

Fig. S19.
Comparison of Q_{st} of C_2H_2 (A) and C_2H_4 (B) adsorption in SIFSIX-1-Cu, SIFSIX-2-Cu, SIFSIX-2-Cu-i, SIFSIX-3-Zn, and SIFSIX-3-Ni and other MOFs.

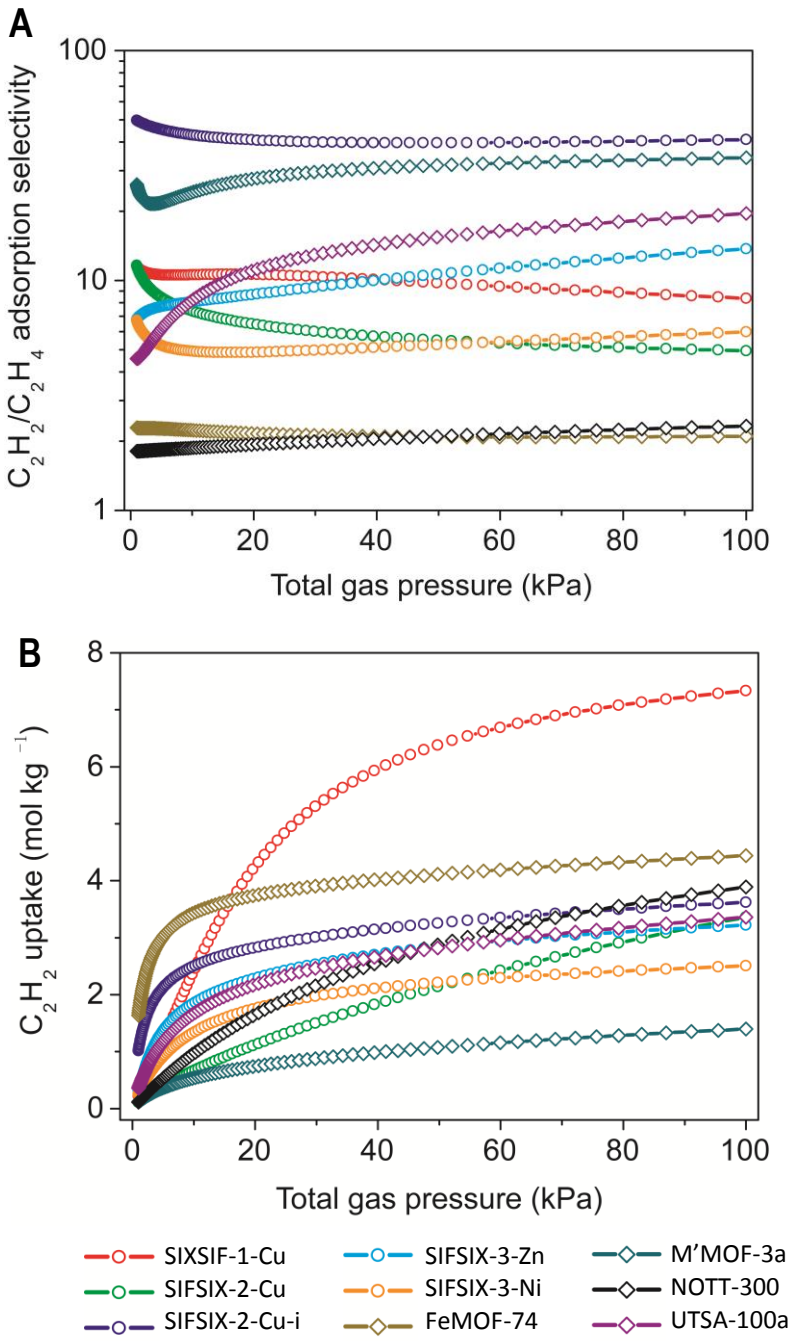

Fig. S20.
IAST calculations of the (A) C_2H_2/C_2H_4 adsorption selectivity, and (B) uptake capacity for adsorption in various MOFs from C_2H_2/C_2H_4 mixtures containing 50% C_2H_2. The data for FeMOF-74 is at a temperature of 318 K; this is the lowest temperature used in the isotherm measurements of Bloch *et al*. (*18*). The data for NOTT-300 is at 293 K (*14*).

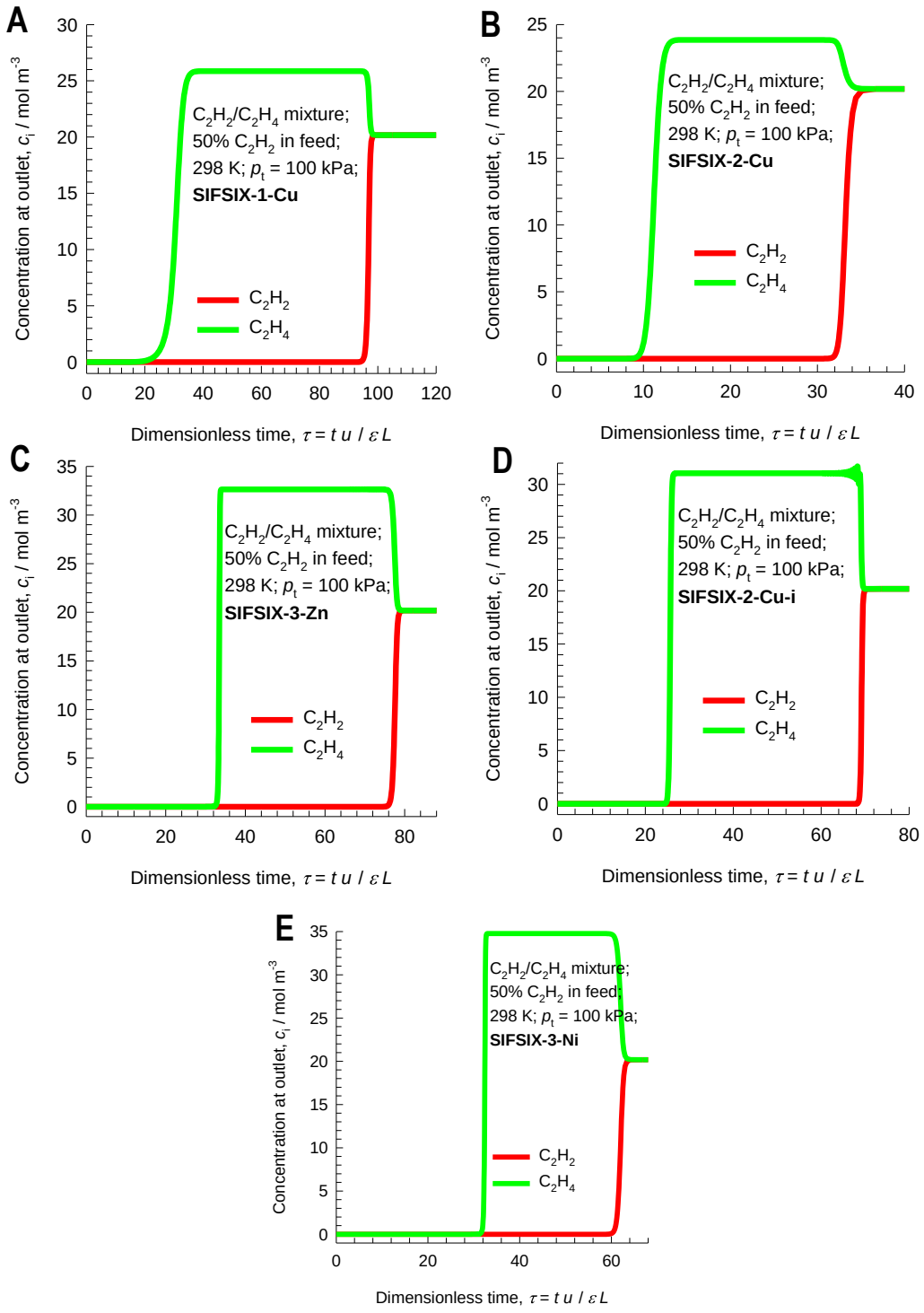

Fig. S21.
Transient breakthrough of C_2H_2/C_2H_4 mixture (50/50, v/v) in an adsorber bed packed SIFSIX-1-Cu (A), SIFSIX-2-Cu (B), SIFSIX-3-Zn (C), SIFSIX-2-Cu-i (D), and SIFSIX-3-Ni (E). The total bulk gas phase is at 298 K and 100 kPa. The partial pressures of C_2H_2, and C_2H_4 in the inlet feed gas mixture are, respectively, p_1 = 50 kPa, p_2 = 50 kPa.

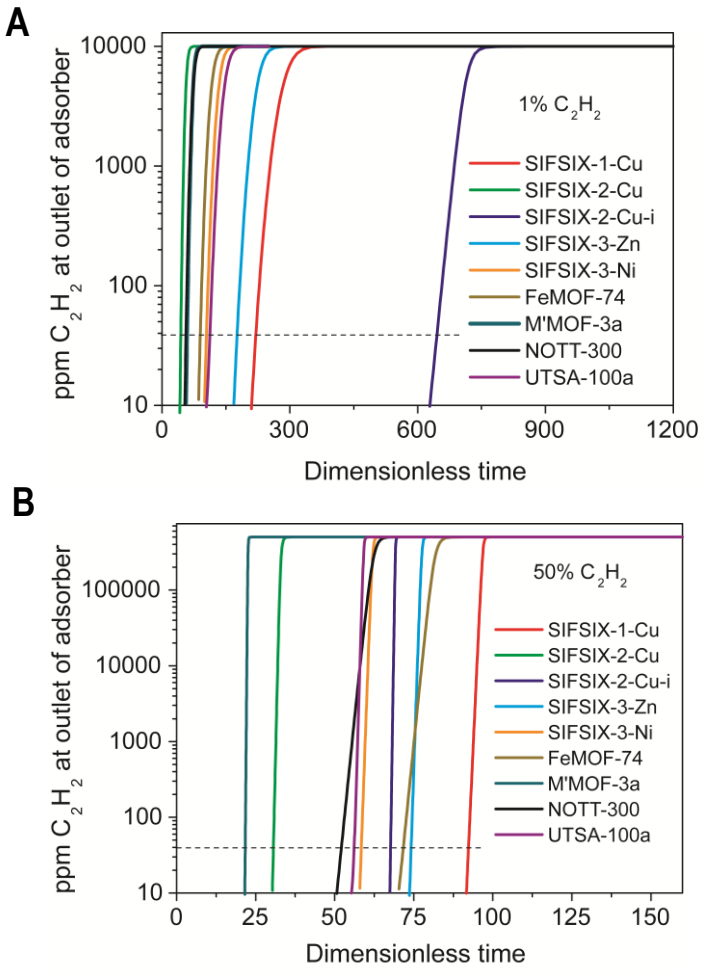

Fig. S22.
Ppm C_2H_2 in the outlet gas of transient breakthrough of C_2H_2/C_2H_4 mixture containing 1% C_2H_2 (A) and 50% C_2H_2 (B) mixture in an adsorber bed packed with various MOFs. At a certain time, τ_{break}, the impurity level will exceed the desired purity level of 40 ppm.

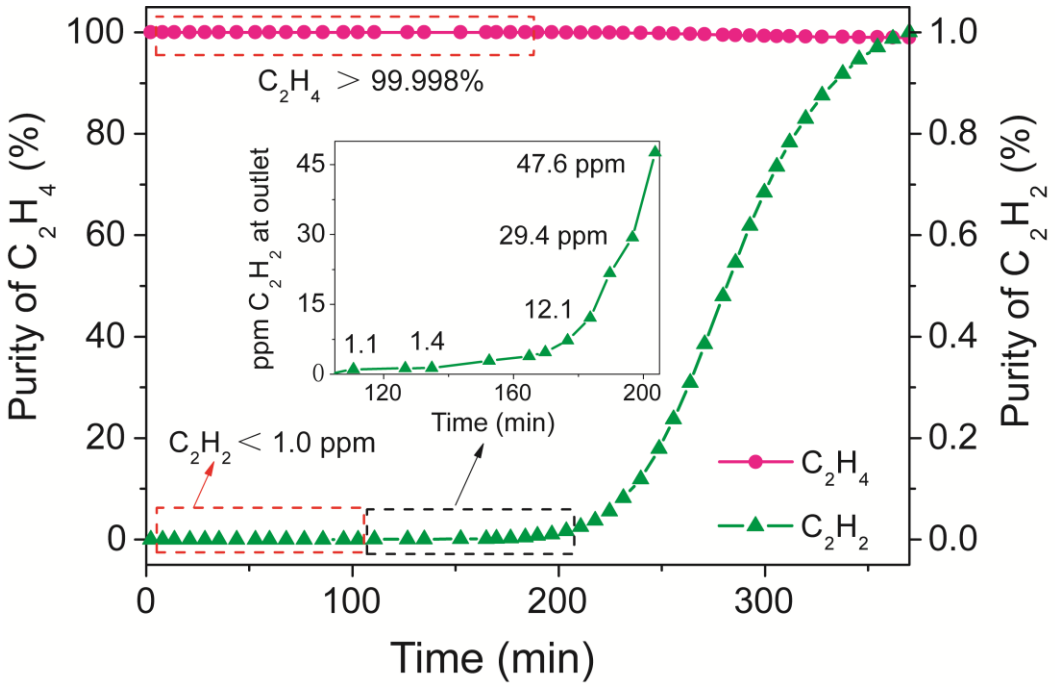

Fig S23.
The concentration of C_2H_2 and the purity of C_2H_4 in the outlet gas of the adsorber. The inserted figure shows the C_2H_2 content in the outlet gas in ppm. Experimental breakthrough was conducted on a stainless steel column packed with SIFSIX-2-Cu-i (Φ4.6×50 mm, 0.21 g SIFSIX-2-Cu-i) with C_2H_2/C_2H_4 mixture (1/99) as feed gas at 1.25 ml/min and 298 K.

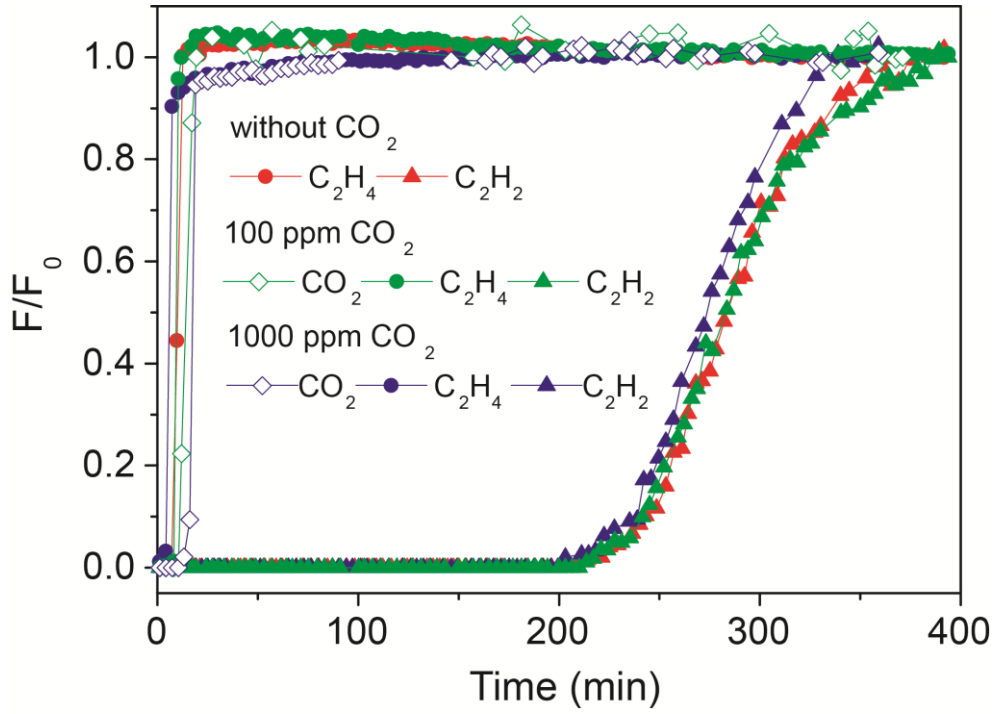

Fig S24.
Experimental column breakthrough curves for C_2H_2/C_2H_4 separations (1/99) on SIFSIX-2-Cu-i at 298 K and 1 atm in the absence and presence of CO_2. (1) 1% C_2H_2 and 99% C_2H_4; (2) 100 ppm CO_2, 1% C_2H_2, and 98.99% C_2H_4; (3) 1000 ppm CO_2, 1% C_2H_2, and 98.9% C_2H_4. The breakthrough experiments were carried out in a column (Φ4.6×50 mm, 0.21 g SIFSIX-2-Cu-i) at a flow rate of 1.25 ml/min.

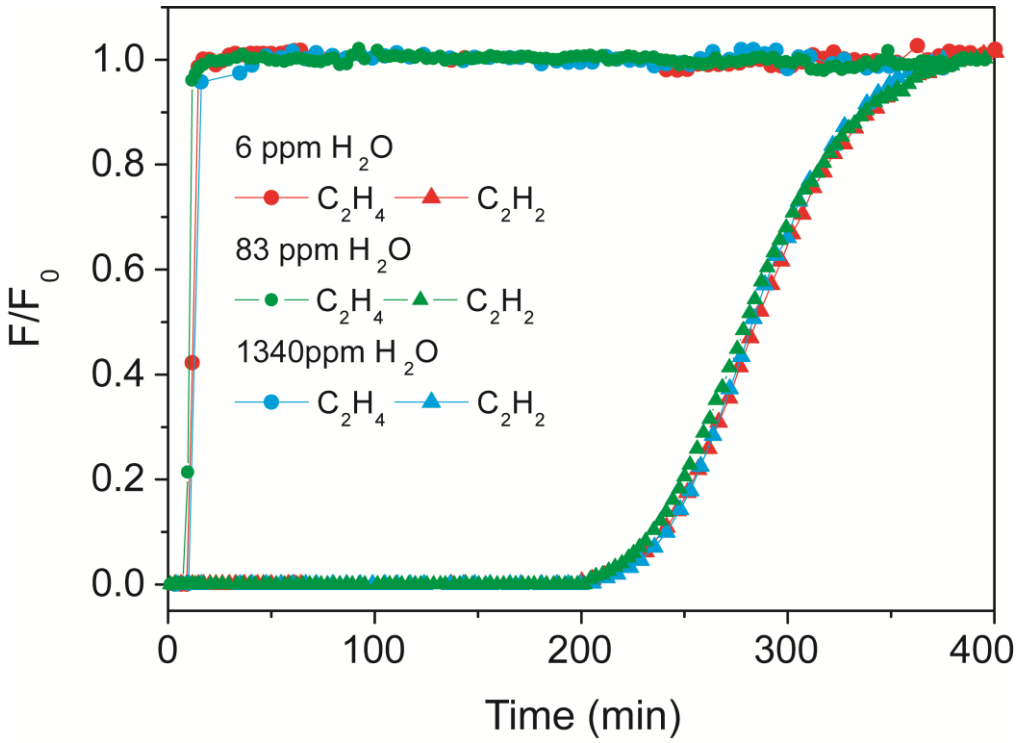

Fig S25.
Experimental column breakthrough curves for C_2H_2/C_2H_4 separations (1/99, v/v) on SIFSIX-2-Cu-i at 298 K and 1 atm with different contents of H_2O. (1) 6 ppm H_2O, 1% C_2H_2 and 98.99% C_2H_4; (2) 83 ppm H_2O, 1% C_2H_2 and 98.99% C_2H_4; (3) 1340 ppm H_2O, 1% C_2H_2 and 98.86% C_2H_4. The breakthrough experiments were carried out in a column (Φ4.6×50 mm, 0.21 g SIFSIX-2-Cu-i) at a flow rate of 1.25 ml/min.

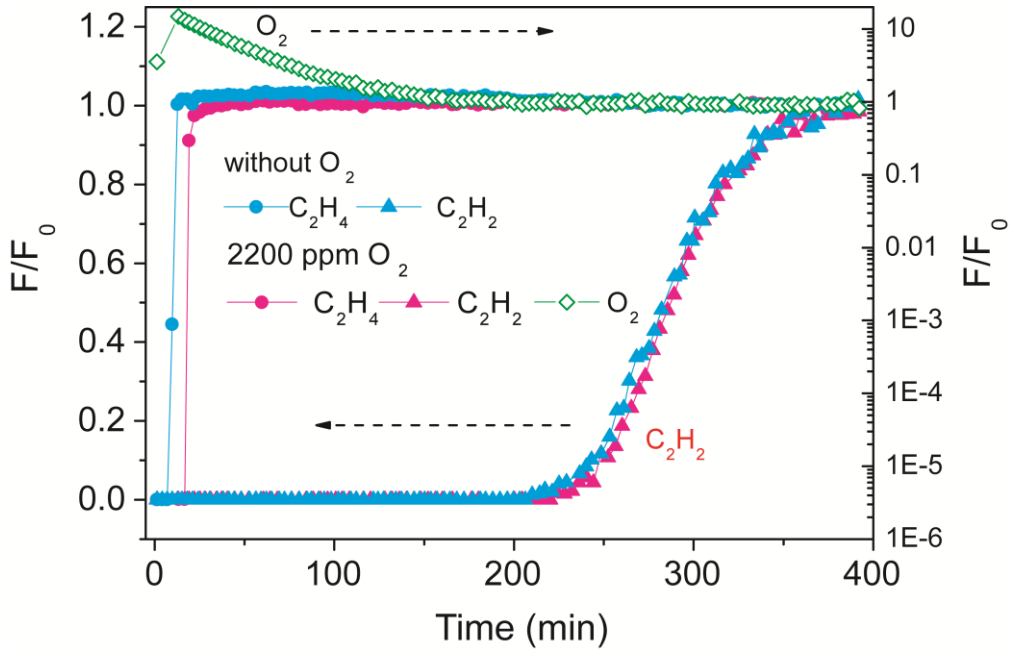

Fig S26.
Experimental column breakthrough curves for C_2H_2/C_2H_4 separations (1/99, v/v) on SIFSIX-2-Cu-i at 298 K and 1 atm with 2200 ppm O_2 and without O_2. The breakthrough experiments were carried out in a column (Φ4.6×50 mm, 0.21 g SIFSIX-2-Cu-i) at a flow rate of 1.25 ml/min.

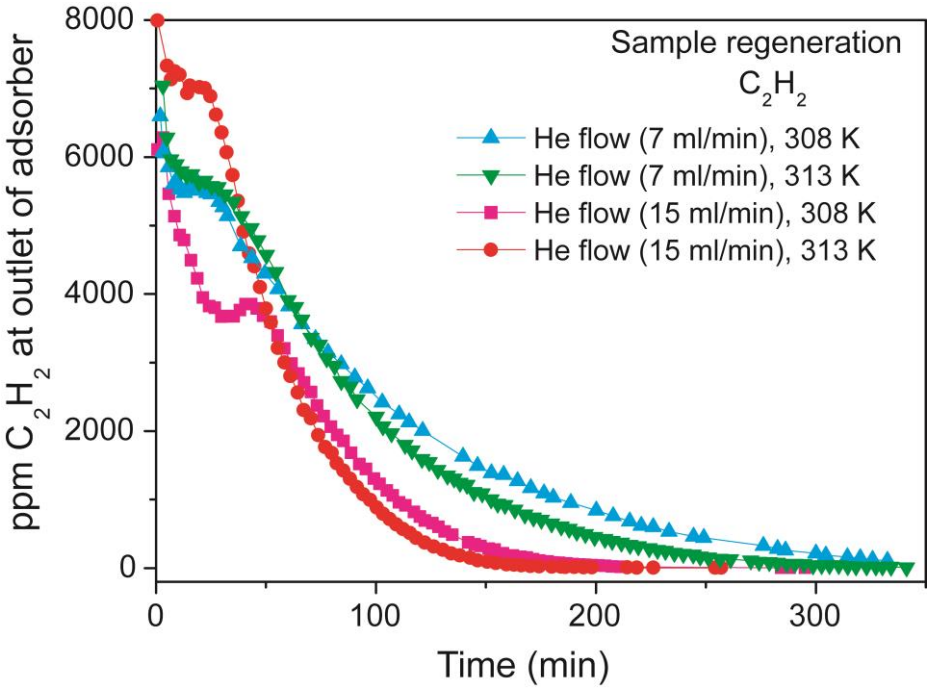

Fig. S27.
Experimental desorption curves for C_2H_2 on SIFSIX-2-Cu-i at different temperatures and He flow rates. Before desorption, the breakthrough experiments for 1/99 C_2H_2/C_2H_4 mixture was carried out in a column (Φ4.6×50 mm, 0.21 g SIFSIX-2-Cu-i) at 298 K.

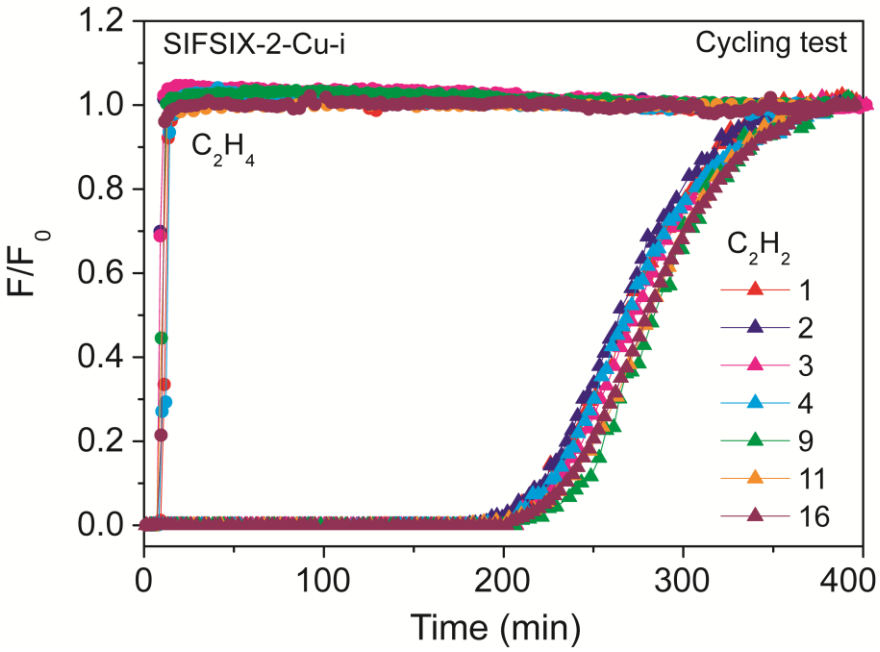

Fig. S28.
Cycling column breakthrough curves for C_2H_2/C_2H_4 separations (1/99, v/v) with SIFSIX-2-Cu-i at 298 K and 1 atm. The breakthrough experiments were carried out in a column (Φ4.6×50 mm, 0.21 g SIFSIX-2-Cu-i) at a flow rate of 1.25 ml/min. Regeneration with He flow (7 to 15 ml/min) for 7 to 12 h at 308 or 313 K. Cycles 1 to 4, 9, 11, and 16 are breakthrough-desorption experiments using C_2H_2/C_2H_4 (1/99) mixtures as feed gases. Cycles 5 to 8 are successive breakthrough-desorption experiments using C_2H_2/C_2H_4 mixtures with different concentrations of CO_2 (fig. S24). Cycle 10 cycle is a breakthrough experiment using C_2H_2/C_2H_4 mixtures with 2200 ppm O_2 (fig. S26). Cycles 12 to 15 are successive breakthrough-desorption experiments using C_2H_2/C_2H_4 mixtures with different concentration of H_2O (fig. S25). The first breakthrough curve (No. 1) was collected three times to ascertain the optimized breakthrough separation parameters.

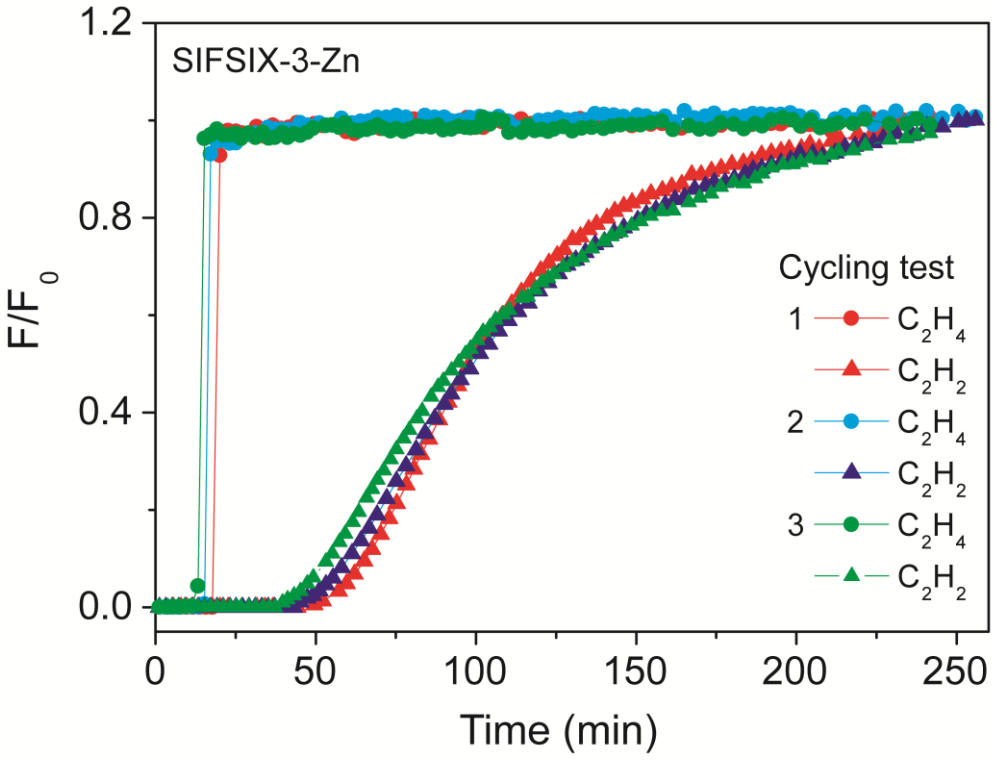

Fig. S29.
Cycling column breakthrough curves for C_2H_2/C_2H_4 separations (1/99, v/v) with SIFSIX-3-Zn at 298 K and 1 atm. The breakthrough experiments were carried out in a column (Φ4.6×50 mm) at a flow rate of 1.25 ml/min. Regeneration with He flow (15 ml/min) for 12 h at 308 K.

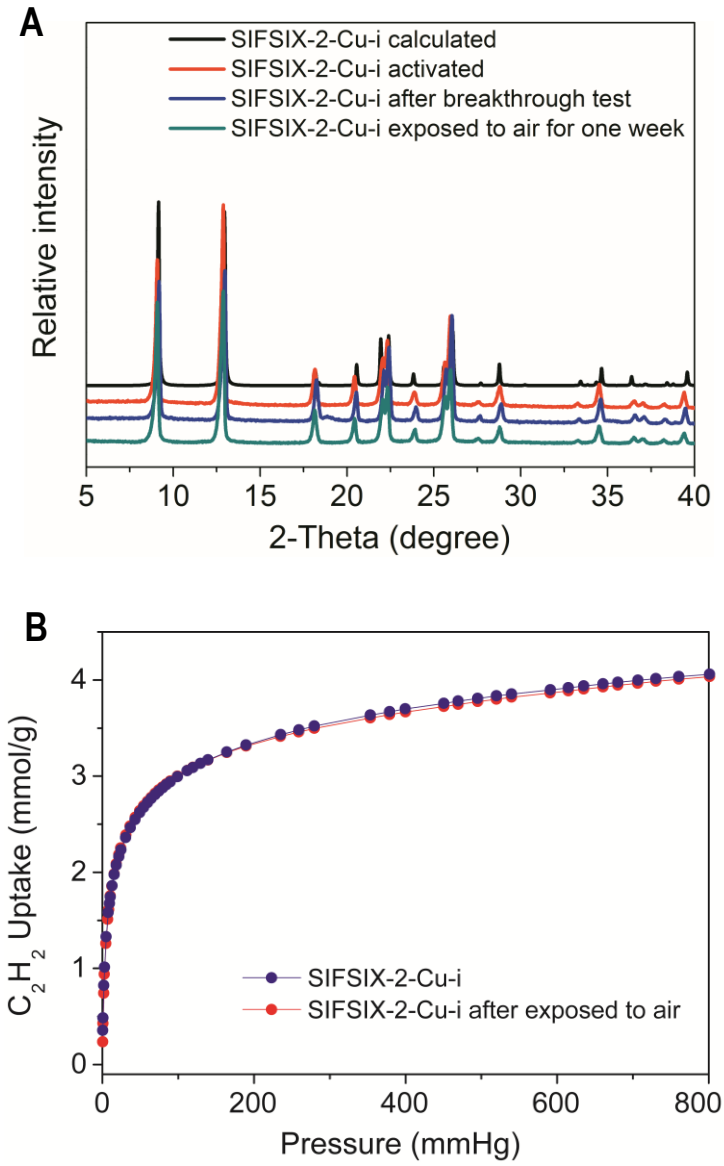

Fig. S30.
(A) XRD patterns of SIFSIX-2-Cu-i after different treatments, and (B) The uptake of C_2H_2 on the SIFSIX-2-Cu-i and the sample after exposure to air for one week with a humidity of 40% to 50 %.

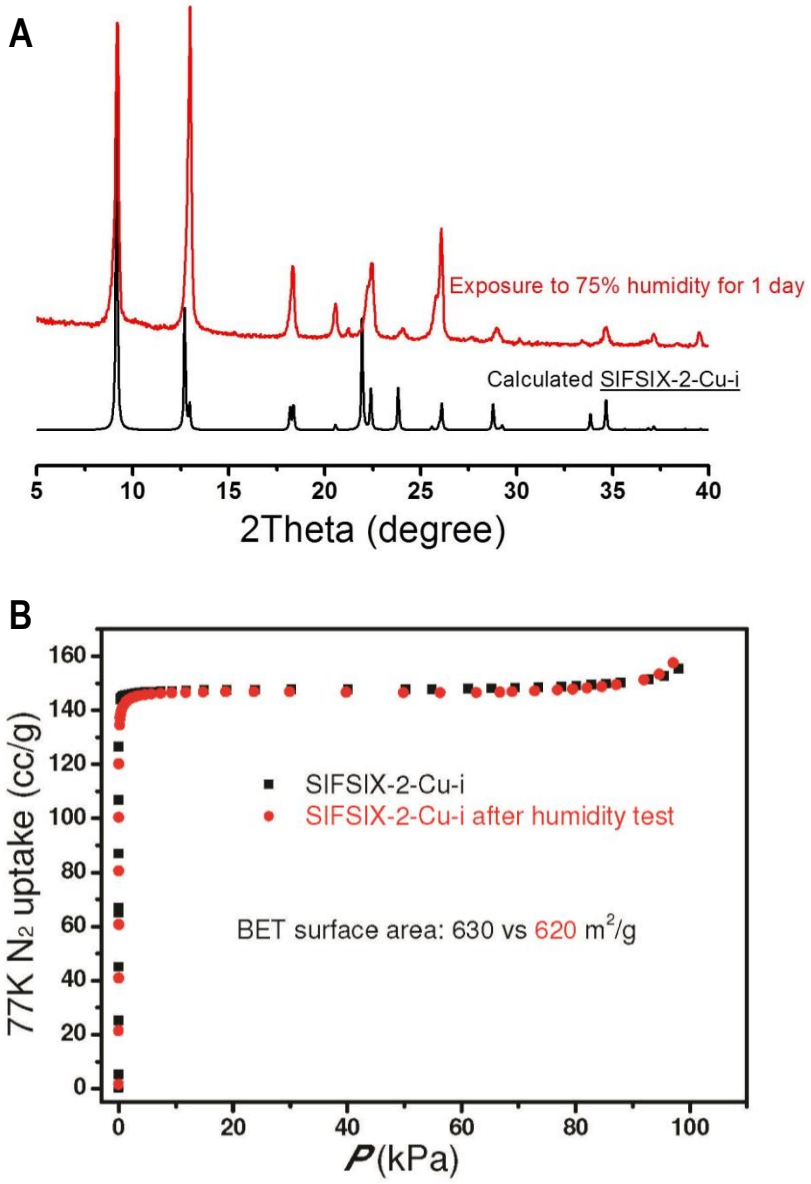

Fig. S31.
(A) XRD patterns of sample SIFSIX-2-Cu-i after exposure to 75% humidity for 1 day. (B) The BET curves of fresh SIFSIX-2-Cu-i and the sample after exposure to 75% humidity for 1 day.

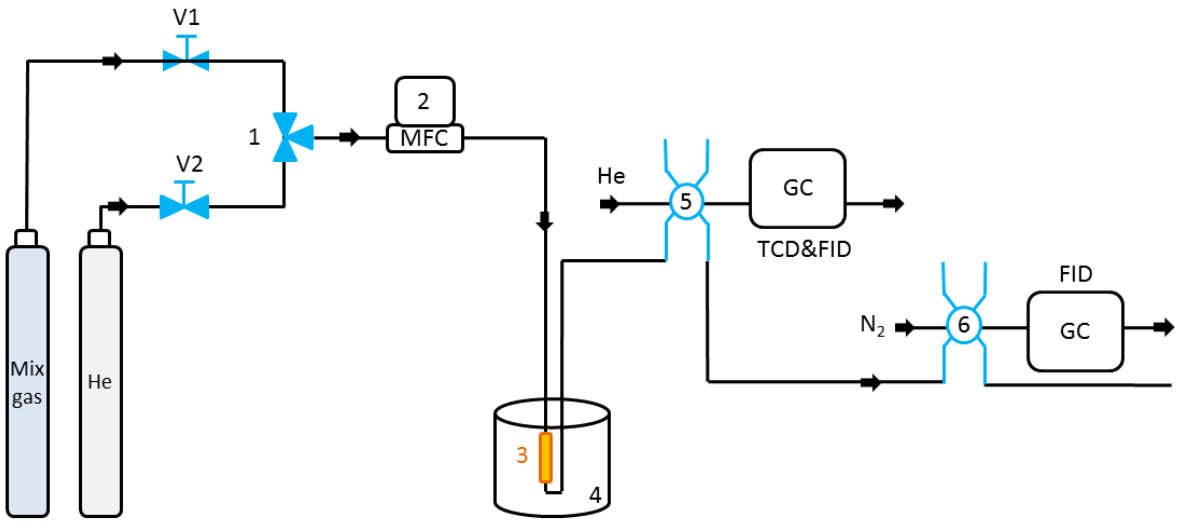

Fig. S32.
Schematic illustration of the apparatus for the breakthrough experiments.

References and Notes

1. S. Kitagawa, Porous materials and the age of gas. *Angew. Chem. Int. Ed.* **54**, 10686–10687 (2015). Medline doi:10.1002/anie.201503835

2. R. Vaidhyanathan, S. S. Iremonger, G. K. Shimizu, P. G. Boyd, S. Alavi, T. K. Woo, Direct observation and quantification of CO_2 binding within an amine-functionalized nanoporous solid. *Science* **330**, 650–653 (2010). Medline doi:10.1126/science.1194237

3. N. T. T. Nguyen, H. Furukawa, F. Gándara, H. T. Nguyen, K. E. Cordova, O. M. Yaghi, Selective capture of carbon dioxide under humid conditions by hydrophobic chabazite-type zeolitic imidazolate frameworks. *Angew. Chem. Int. Ed.* **53**, 10645–10648 (2014). Medline doi:10.1002/ange.201403980

4. N. L. Rosi, J. Eckert, M. Eddaoudi, D. T. Vodak, J. Kim, M. O'Keeffe, O. M. Yaghi, Hydrogen storage in microporous metal-organic frameworks. *Science* **300**, 1127–1129 (2003). Medline doi:10.1126/science.1083440

5. Y. Peng, V. Krungleviciute, I. Eryazici, J. T. Hupp, O. K. Farha, T. Yildirim, Methane storage in metal-organic frameworks: Current records, surprise findings, and challenges. *J. Am. Chem. Soc.* **135**, 11887–11894 (2013). Medline doi:10.1021/ja4045289

6. J. A. Mason, J. Oktawiec, M. K. Taylor, M. R. Hudson, J. Rodriguez, J. E. Bachman, M. I. Gonzalez, A. Cervellino, A. Guagliardi, C. M. Brown, P. L. Llewellyn, N. Masciocchi, J. R. Long, Methane storage in flexible metal-organic frameworks with intrinsic thermal management. *Nature* **527**, 357–361 (2015). Medline doi:10.1038/nature15732

7. S. Ma, D. Sun, J. M. Simmons, C. D. Collier, D. Yuan, H. C. Zhou, Metal-organic framework from an anthracene derivative containing nanoscopic cages exhibiting high methane uptake. *J. Am. Chem. Soc.* **130**, 1012–1016 (2008). Medline doi:10.1021/ja0771639

8. H. Furukawa, K. E. Cordova, M. O'Keeffe, O. M. Yaghi, The chemistry and applications of metal-organic frameworks. *Science* **341**, 1230444 (2013). Medline

9. S. J. Datta, C. Khumnoon, Z. H. Lee, W. K. Moon, S. Docao, T. H. Nguyen, I. C. Hwang, D. Moon, P. Oleynikov, O. Terasaki, K. B. Yoon, CO_2 capture from humid flue gases and humid atmosphere using a microporous coppersilicate. *Science* **350**, 302–306 (2015). Medline doi:10.1126/science.aab1680

10. Z. J. Zhang, Z.-Z. Yao, S. Xiang, B. Chen, Perspective of microporous metal–organic frameworks for CO_2 capture and separation. *Energy Environ. Sci.* **7**, 2868–2899 (2014). doi:10.1039/C4EE00143E

11. Q. Lin, T. Wu, S. T. Zheng, X. Bu, P. Feng, Single-walled polytetrazolate metal-organic channels with high density of open nitrogen-donor sites and gas uptake. *J. Am. Chem. Soc.* **134**, 784–787 (2012). Medline doi:10.1021/ja2092882

12. J.-R. Li, R. J. Kuppler, H.-C. Zhou, Selective gas adsorption and separation in metal-organic frameworks. *Chem. Soc. Rev.* **38**, 1477–1504 (2009). Medline doi:10.1039/b802426j

13. R. Matsuda, R. Kitaura, S. Kitagawa, Y. Kubota, R. V. Belosludov, T. C. Kobayashi, H. Sakamoto, T. Chiba, M. Takata, Y. Kawazoe, Y. Mita, Highly controlled acetylene

accommodation in a metal-organic microporous material. *Nature* **436**, 238–241 (2005). Medline doi:10.1038/nature03852

14. S. Yang, A. J. Ramirez-Cuesta, R. Newby, V. Garcia-Sakai, P. Manuel, S. K. Callear, S. I. Campbell, C. C. Tang, M. Schröder, Supramolecular binding and separation of hydrocarbons within a functionalized porous metal-organic framework. *Nat. Chem.* **7**, 121–129 (2014). Medline doi:10.1038/nchem.2114

15. H. Wu, Q. Gong, D. H. Olson, J. Li, Commensurate adsorption of hydrocarbons and alcohols in microporous metal organic frameworks. *Chem. Rev.* **112**, 836–868 (2012). Medline doi:10.1021/cr200216x

16. J.-P. Zhang, X.-M. Chen, Optimized acetylene/carbon dioxide sorption in a dynamic porous crystal. *J. Am. Chem. Soc.* **131**, 5516–5521 (2009). Medline doi:10.1021/ja8089872

17. T. L. Hu, H. Wang, B. Li, R. Krishna, H. Wu, W. Zhou, Y. Zhao, Y. Han, X. Wang, W. Zhu, Z. Yao, S. Xiang, B. Chen, Microporous metal-organic framework with dual functionalities for highly efficient removal of acetylene from ethylene/acetylene mixtures. *Nat. Commun.* **6**, 7328–7335 (2015). Medline doi:10.1038/ncomms8328

18. E. D. Bloch, W. L. Queen, R. Krishna, J. M. Zadrozny, C. M. Brown, J. R. Long, Hydrocarbon separations in a metal-organic framework with open iron(II) coordination sites. *Science* **335**, 1606–1610 (2012). Medline doi:10.1126/science.1217544

19. M. C. Das, Q. Guo, Y. He, J. Kim, C. G. Zhao, K. Hong, S. Xiang, Z. Zhang, K. M. Thomas, R. Krishna, B. Chen, Interplay of metalloligand and organic ligand to tune micropores within isostructural mixed-metal organic frameworks (M'MOFs) for their highly selective separation of chiral and achiral small molecules. *J. Am. Chem. Soc.* **134**, 8703–8710 (2012). Medline doi:10.1021/ja302380x

20. P. Nugent, Y. Belmabkhout, S. D. Burd, A. J. Cairns, R. Luebke, K. Forrest, T. Pham, S. Ma, B. Space, L. Wojtas, M. Eddaoudi, M. J. Zaworotko, Porous materials with optimal adsorption thermodynamics and kinetics for CO_2 separation. *Nature* **495**, 80–84 (2013). Medline doi:10.1038/nature11893

21. S. Noro, R. Kitaura, M. Kondo, S. Kitagawa, T. Ishii, H. Matsuzaka, M. Yamashita, Framework engineering by anions and porous functionalities of Cu(II)/4,4′-bpy coordination polymers. *J. Am. Chem. Soc.* **124**, 2568–2583 (2002). Medline doi:10.1021/ja0113192

22. O. Shekhah, Y. Belmabkhout, Z. Chen, V. Guillerm, A. Cairns, K. Adil, M. Eddaoudi, Made-to-order metal-organic frameworks for trace carbon dioxide removal and air capture. *Nat. Commun.* **5**, 4228–4234 (2014). Medline doi:10.1038/ncomms5228

23. A. Kumar, D. G. Madden, M. Lusi, K.-J. Chen, E. A. Daniels, T. Curtin, J. J. Perry 4th, M. J. Zaworotko, Direct air capture of CO_2 by physisorbent materials. *Angew. Chem. Int. Ed.* **54**, 14372–14377 (2015).doi:10.1002/anie.201506952 Medline

24. Materials and methods are available as supplementary materials on *Science* Online.

25. F. Studt, F. Abild-Pedersen, T. Bligaard, R. Z. Sørensen, C. H. Christensen, J. K. Nørskov, Identification of non-precious metal alloy catalysts for selective hydrogenation of acetylene. *Science* **320**, 1320–1322 (2008). Medline doi:10.1126/science.1156660

26. K. S. Walton, D. S. Sholl, Predicting multicomponent adsorption: 50 years of the ideal adsorbed solution theory. *AIChE J.* **61**, 2757–2762 (2015). doi:10.1002/aic.14878

27. R. Krishna, Methodologies for evaluation of metal–organic frameworks in separation applications. *RSC Adv.* **5**, 52269–52295 (2015). doi:10.1039/C5RA07830J

28. K. M. Sundaram, M. M. Shreehan, E. F. Olszewski, "Ethylene," in *Kirk-Othmer Encyclopedia of Chemical Technology* (Wiley Online Library, 2001).

29. A. C. Larson, R. B. Von Dreele, *General Structure Analysis System* (LAUR 86-748, Los Alamos National Laboratory, 1994).

30. V. Barone, M. Casarin, D. Forrer, M. Pavone, M. Sambi, A. Vittadini, Role and effective treatment of dispersive forces in materials: Polyethylene and graphite crystals as test cases. *Comput. Chem.* **30**, 934–939 (2009). Medline doi:10.1002/jcc.21112

31. R. T. Yang, *Gas Separation by Adsorption Processes* (Butterworth Publishers, 1986).

32. Y.-B. He, R. Krishna, B. Chen, Metal-organic frameworks with potential for energy-efficient adsorptive separation of light hydrocarbons. *Energy Environ. Sci.* **10**, 9107–9120 (2012). doi:10.1039/c2ee22858k

33. R. Krishna, The Maxwell-Stefan description of mixture diffusion in nanoporous crystalline materials. *Microporous Mesoporous Mater.* **185**, 30–50 (2014). doi:10.1016/j.micromeso.2013.10.026

34. S. D. Burd, S. Ma, J. A. Perman, B. J. Sikora, R. Q. Snurr, P. K. Thallapally, J. Tian, L. Wojtas, M. J. Zaworotko, Highly selective carbon dioxide uptake by [Cu(bpy-*n*)$_2$(SiF$_6$)] (bpy-1 = 4,4′-bipyridine; bpy-2 = 1,2-bis(4-pyridyl)ethene). *J. Am. Chem. Soc.* **134**, 3663–3666 (2012). Medline doi:10.1021/ja211340t